LATERAL CAPACITY OF SUCTION CAISSONS IN BILINEAR SOIL SYSTEM

A Thesis

by

ADNAN ASHRAF

Submitted to the Office of Graduate and Professional Studies of
Texas A&M University
in partial fulfillment of the requirements for the degree of

MASTER OF SCIENCE

Chair of Committee,	Charles Aubeny
Committee Members,	Zenon Medina-Cetina
	Julia Reece
Head of Department,	Robin Autenrieth

August 2018

Major Subject: Civil Engineering

ABSTRACT

Suction caisson anchors have been proven as efficient and cost-effective foundations for offshore wind turbines. These anchors are subjected to lateral loads which are typical of offshore environment. Many efforts have been made to determine the ultimate lateral capacity of the soil around caissons. Upper bound plastic limit analysis provides a useful framework to estimate the lateral capacity under undrained conditions. A three-dimensional collapse mechanism is assumed by defining four optimization parameters along the geometry of the failure, and ultimate capacity is determined by optimizing the parameters. This method is able to incorporate the soil complexities and has been successfully used in industry for years. But the drawback of the approach is that it requires a lot of computational effort due to the optimization parameters involved. A computationally more efficient method has been devised by reducing the optimization parameters from four to one. However, the expedient restricts the method to analysis of caissons in uniform or linearly varying undrained strengths. In reality, offshore soils are different from strength profile of uniform or linearly varying strength. This research is aimed to develop a methodology which could make the simplified method applicable for bilinear soil strength system. An equivalent strength profile is proposed which, in turn, is used in the simplified method for the estimation of ultimate capacity. The results are validated by the upper bound plastic limit analysis. In the end, series of parametric studies are performed to affirm the validation of the proposed methodology.

ACKNOWLEDGEMENTS

It has been a privilege to work under the supervision of Dr. Charles Aubeny. I thank him for his guidance and assistance he provided throughout the course of the research.

I would also like to thank Dr. Zenon Medina-Cetina and Dr. Julia Reece for contributing as committee members.

Special thanks to Francisco Grajales and Brian Diaz for the support provided in the initial stage of coding.

I would also like to thank the staff at Zachary Department of Civil Engineering for all the support they provided during my time as student.

To my parents, Javeda and Ashraf, I can never thank enough for their unconditional love and prayers, without which I could never come so far.

TABLE OF CONTENTS

LIST OF FIGURES

Page

LIST OF TABLES

Page

1 INTRODUCTION

1.1 Offshore Geotechnical Engineering

With the growing demand for energy, construction of offshore structures is on rise. Offshore geotechnical engineering evolved from onshore practices, but over the period of time, the two fields have taken a different course due to the difference in type of structures, and construction and installation procedures (Randolph et al., 2011). These structures are not only different than onshore structures but they are also exposed to a set of unique environmental loads. Some of these loads are tidal loads (waves and sea-currents), earthquakes and tsunamis, and wind loads (Gerwick., 2000).

Both horizontal and vertical loads act on offshore structures. Three broad categories of the loads acting on offshore structures are made (Bai & Bai, 2012): (1) Permanent loads—the loads that do not vary for an extended period of time in terms of magnitude and point of application, (2) Live and dynamic loads—loads applied during the installation of the structure and vary in magnitude and application point, and (3) Environmental loads—loads carrying the environmental effects and can be steady or cyclic in nature.

Loads are normally applied to the structure and then transmitted to the foundation. Therefore, they are not only considered for the structural design of super-structures but are also taken into account in the foundation design.

1.2 Offshore Structures and Foundations

The offshore structures were traditionally associated with oil and gas industry. Astronomical platforms, having major loads acting in vertical direction are typical oil-gas

structures. To transfer the load safely to subsea soil, gravity structures are the foremost structures built. However, due to their high cost, other alternatives were sought. The typical offshore oil and gas structure are shown in Figure 1.1.

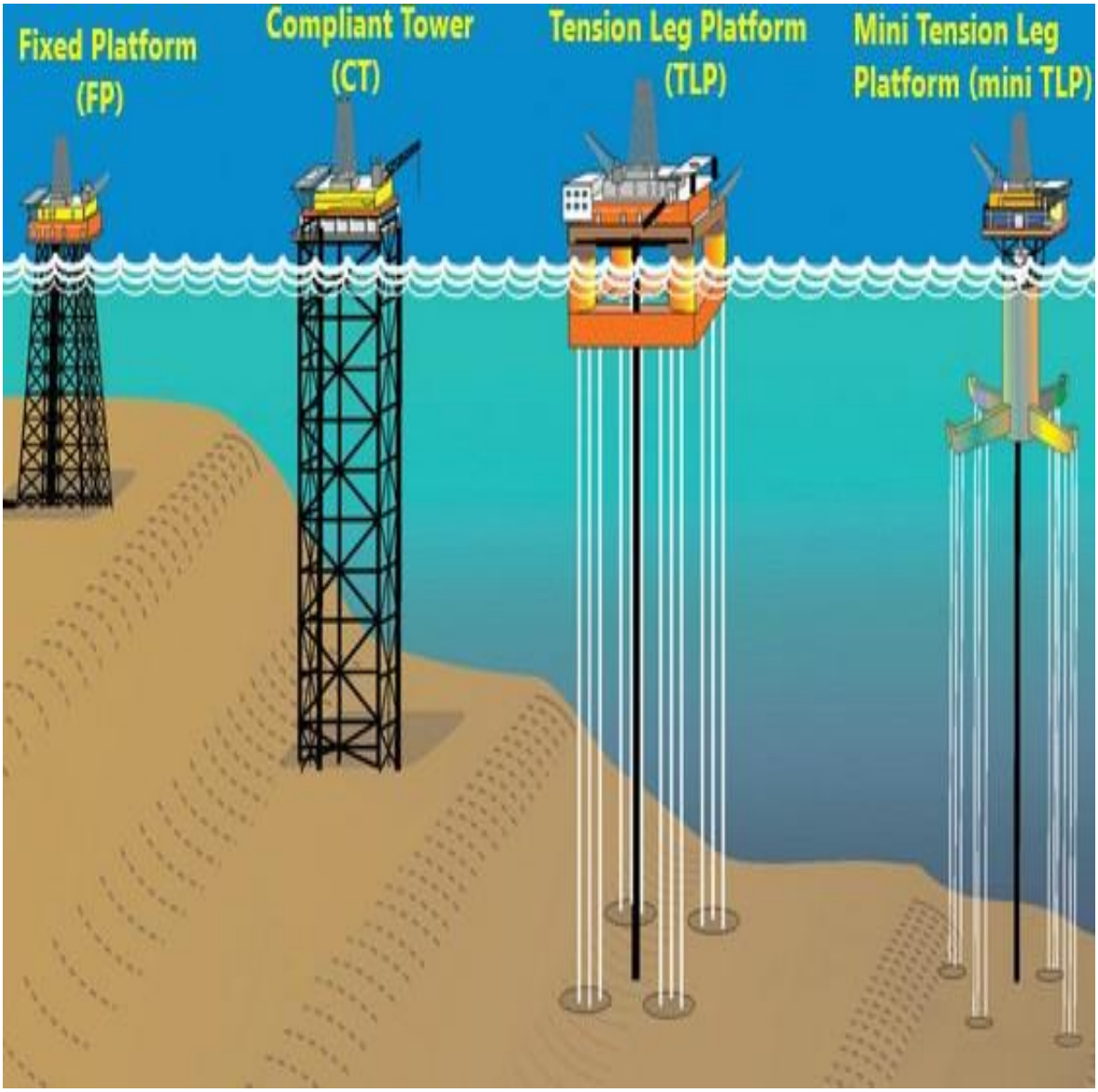

Figure 1. 1: Typical oil and gas platform supporting structures (Source: The Bureau of Ocean Engineering Management)

Due to a worldwide push for clean energy, wind energy generation facilities are growing. However, they require a vast stretch of land if built onshore. Offshore wind turbines not only address this issue but offshore also offers superior wind corridors for energy generation. Moreover, larger wind turbines are normally built in offshore areas due to low installation and maintenance cost which, in turn, provides the benefit of lower energy cost (Arapogianni et al., 2013).

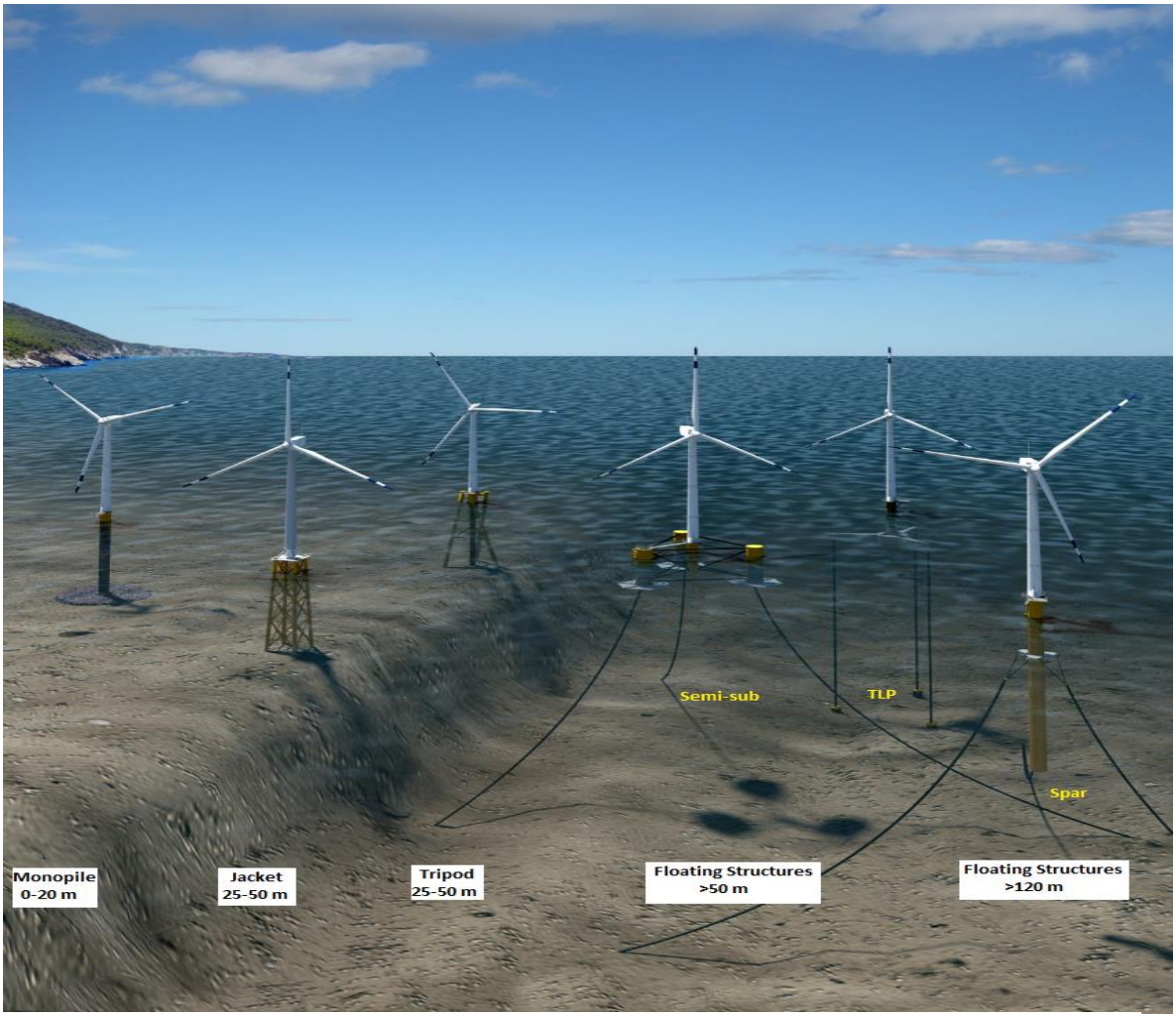

Figure 1. 2: Typical offshore wind turbine foundations (Source: US Department of Energy)

Offshore wind turbine foundations are of many different types, consisting of fixed structures i.e. simple monopoles and tripod/jacket, and anchors connected to floating

structures. Environmental loads, generation capacity, and depth of water as well as offshore geotechnical investigation of soil along with the type and magnitude of forces are the deciding factors for the type of foundation required. Figure 1.2 shows the typical foundation structures built for offshore wind turbines. These structures are much smaller and lighter in weight compared to typical oil and gas platforms. Therefore, horizontal loads and overturning moments are much larger than vertical loads for these structures.

Over the past few years floating wind turbines have gained more popularity. They offer a number of advantages over other available options since they are cost effective, simple to install, enable access to remote offshore areas, and eliminate the need to design the piece between water level and foundation (Roddier et al., 2010). Moreover, fixed foundations are only valid for turbines within 5 m water depth whereas monopoles are limited to 20 m (Li et al., 2015). The solution for wind turbines foundation in deep water was sought in the form of floating wind turbine with a suction anchor connected to base of turbine tower by mooring lines.

1.2.1 Suction Anchors

A suction anchor is a hollow steel pile closed at top and open-ended at bottom. They are large in diameter and length to diameter (L_f/D) ratio is typically 6 or less (Randolph et al., 2011). Mooring lines are attached to the anchors on the side (Figure 1.3).

As the name suggests, suction caissons are installed by producing a negative pressure (suction). They are dropped to the sea-bed and initial penetration is caused by self-weight. Suction induced by pumping water out from inside of caisson creates a differential pressure across the top cap of the caisson. With sufficient pressure the net force acting on the caisson can overcome the undrained shear strength of the soil, allowing the

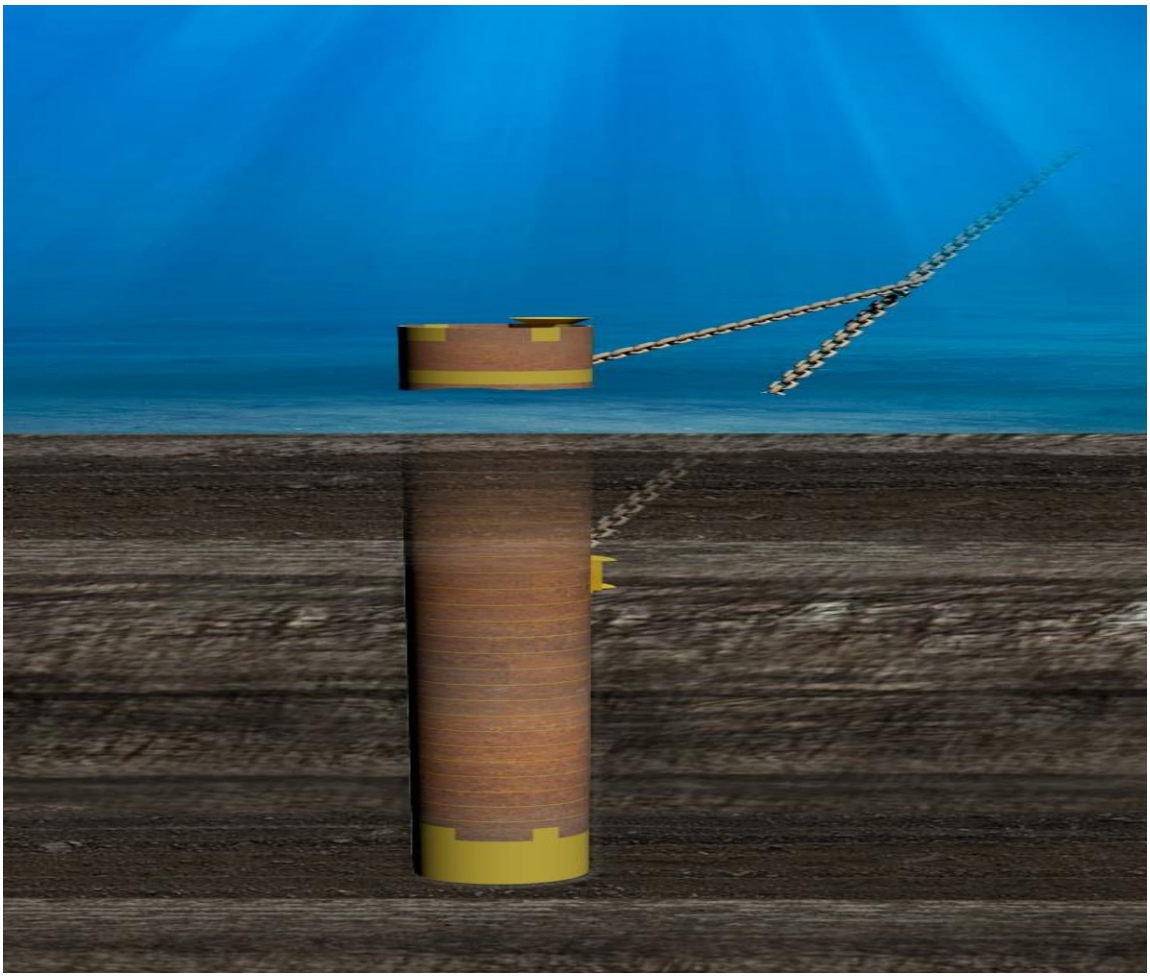

Figure 1. 3: A suction caisson with mooring line attached (Source: US Department of Energy)

caisson to advance to its design depth. Once the caisson is penetrated into the soil, it has capability to resist both axial and lateral loads, hence, can be used as pile foundation or anchors. Figure 1.4 shows a schematic illustration of suction caisson installation. An

opening is made in the lid to attach a pump for drawing water out. As the water moves out from caisson, it penetrates into the sea-bed. This method of installation is generally applicable to cohesive soil while in sandy soils, it has shown poor performance.

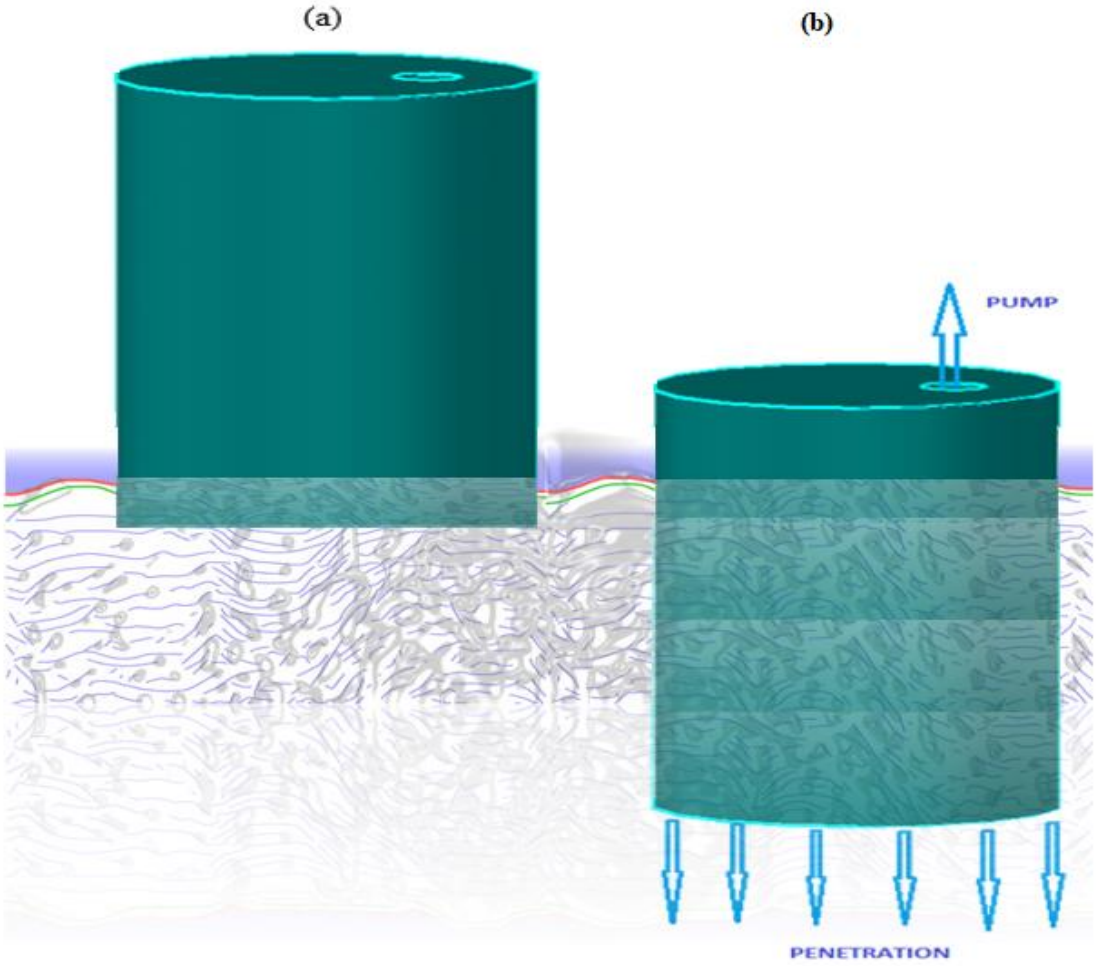

Figure 1. 4: Schematic diagram of suction caisson installation (a) Caisson at sea-bed, (b) Caisson penetrating under the suction

Suction caissons have gained popularity in recent years due to their number of advantages over conventional deep foundations. The main benefits are as below:

1. Suction caissons are generally larger in diameter than driven piles hence capable of resisting larger loads.
2. Their installation procedure is easy and cost effective.

3. They are mostly used as anchors for floating platforms, but can be used as vertically loaded piles where their installation procedure is applicable.
4. Their movement is easy and less expensive since they are much lighter in weight compared mono-piles.
5. They can be easily retrieved by reversing the installation process.
6. They can be re-used after decommissioning.

1.3 Methods of Analysis of Suction Caissons

Suction caissons, when installed can be used as conventional pile foundation or anchors for a floating platform. In the former case they are subjected to vertical loads and moments whereas they have to resist horizontal loads and moments—applied through mooring lines—when used as anchors.

Exact analytical solutions for the analysis of laterally loaded piles are very difficult due to the complexity of failure mechanism. Researchers have proposed approximate as well as some empirical solutions for the analysis. Finite element method can also be used as an alternative for the analysis.

The approximate solution which has enjoyed significant popularity in industry and is very versatile in nature is proposed by Murff & Hamilton (1993)—famously known as Murff-Hamilton Plastic Limit Analysis. The method is based on theoretical solution of the failure mechanism which is proven by experimental evidence. The method parameters associated with the geometry of failure mechanism to analyze the capacity of piles. A major advantage of the method is that it is capable of incorporating complex geometries and varying material properties. However, it takes a significant computational effort since it

involves volume and surface integrals as well as optimization of the parameters. Another disadvantage of the method is that it has shown unreliable results for short piles.

Empirical solution, also known as Simplified Analysis however, has great computational efficiency. It is simple to understand and can be used in the form of spread sheet. However, the solution is limited to uniform or linearly varying strength profiles.

Finite element solution has an advantage over the above methods in the sense that it can be applied to pile of any aspect ratio and complex soils. The disadvantage of the method is that it also involves significant computation. Moreover, limitations on the degree of mesh refinement needed to achieve accurate solutions, particularly for three-dimensional problems, generally lead to over-estimation of ultimate load capacity from the finite element method.

1.4 Study Problem

Many researchers have reported stratified sea-bed at various locations around the world (Baglioni et al., 1982, Sættem et al., 1996, Koutsoftas et al., 1987, Young et al., 1984). The layering is attributed to gradual deposition of soils spanning over millions of years. A soil profile of bilinear strength gradient is commonly found in Gulf of Maine, Gulf of Mexico, offshore areas in Hong Kong, and Norway. The effect of layering should be considered while predicting the capacity of piles and caissons in such soils.

The simplified method is highly desirable due its computational simplicity. Since the method is limited to uniform or linearly varying soil strength profiles, efforts are needed to develop a methodology that could make the method applicable to bilinear soil system.

1.4.1 Simplified Analysis for Lateral Capacity in Bilinear Soil System

The basic reason that the simplified method is not applicable to nonlinear soil strength is that it depends on an empirical factor N_p proposed by Murff & Hamilton (1993). The factor is limited to uniform or linearly varying soil profiles. To use the simplified method in current form, bilinear soil profiles will be modified into equivalent linear profiles. If the method proved as grossly inaccurate, a modified empirical factor based on bilinear soil case would be proposed. Extensive analysis will be carried out to verify the reliability of proposed methodology by various parametric studies. Limitations of the method (if any) will also be pointed out.

2 LITERATURE REVIEW

2.1 Soil Models

With the development of finite element and finite difference method it is now possible to analyze complex geotechnical structures. The methods require input on how soil will behave under the action of load. These behaviors are incorporated by specifying a soil model available in the finite element programs. By definition, a soil model is a mathematical representation of soil behavior under the application of load. The onset of development of theoretical soil models dates back to eighteenth century (1773) when Coulomb first presented a soil failure mechanism (Heyman, 1972). Around the end of nineteenth century, Mohr expanded it to a more generalized form which today is known as Mohr-Coulomb theory (Yu & M.-h., 2002). Based on stress strain behavior in triaxial test in drained conditions, Duncan & Chang (1970) presented another soil model which is popular in United States as nonlinear model. Similarly, another model was presented at Cambridge University by Schofield & Wroth (1968) which is based on behavior of normally consolidated cohesive soils when subjected to triaxial compression test. The model was later modified, hence known as Modified Cam-Clay model. All these models are based on theoretical explanation of how a material behaves under the action of load, commonly known as strength theories. The strength theory which encompasses the explanation of behavior of geotechnical engineering structures is known as theory of plasticity.

Materials normally show strain hardening or softening behavior due to rearrangement of particles but for simplicity many models assume a purely plastic

behavior. The best model for soil is not necessarily the one which precisely fits with the experimental results (Houlsby, 1981). Soil is a very complex material and a more accurate model need more parameters which are likely to be difficult to obtain, hence making the model complex. Complex models have another disadvantage that they are very unlikely to provide a rational explanation of soil behavior. A simple model, on other hand, have many advantages which might outweigh the loss of precision.

2.2 Plasticity Theory

In plasticity theory, the material is presented as an idealized material that shows elastic strain up to a certain stress state (called yield point) and then a combination of elastic and plastic or purely plastic strain is assumed. Like any other theory, in plasticity theory there are few assumptions which were made prior to development. Firstly, the material is assumed to be isotropic, that is, at any point the material properties are same in all directions. Secondly, strain rate and thermal effects of loading are neglected. The purpose of plasticity theory was twofold: (1) to propose a relationship for stress and strain which could agree closely and universally with observations as need be, and (2) to postulate a mathematical procedure for plastic deformations in materials (Hill, 1998). Following through the goal, the theory was fragmented into following components:

1- Yield criteria and yield locus

2- Plastic flow rule

3- Hardening laws

4- Behavior within elastic range

Yield Criteria and Flow Rule are bases of plastic limit analysis hence they are discussed in detail in following sections.

2.3 Yield Criteria and Yield Locus

Suppose that a material is subjected to uniaxial stress as shown in Figure 2.1. The material initially shows elastic behavior, that is, if the load is removed the material returns to its original shape.

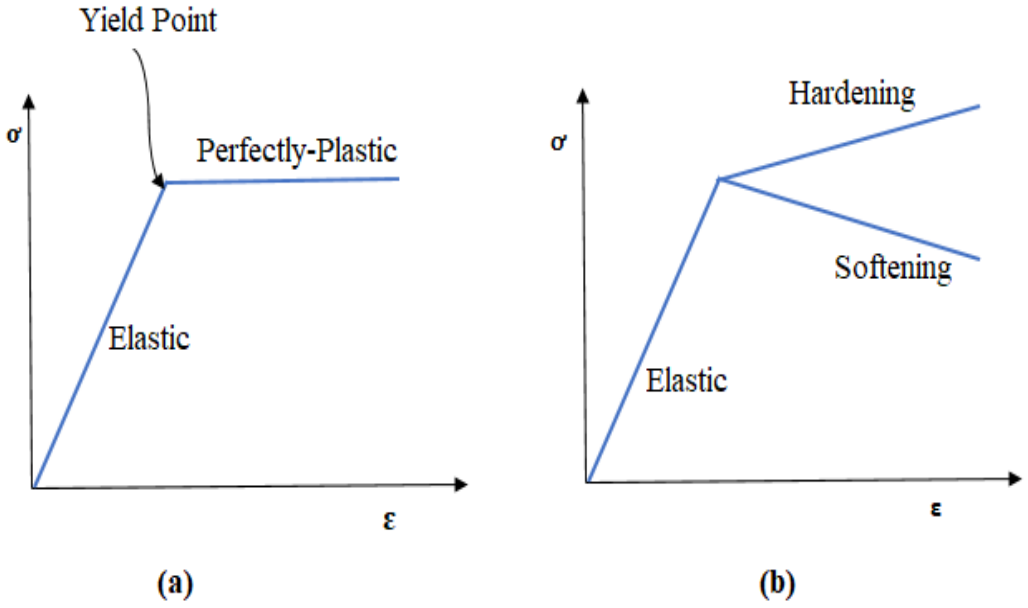

Figure 2. 1: Material subjected to uniaxial stress system (a) Elastic perfectly plastic material (b) Elastic-plastic material

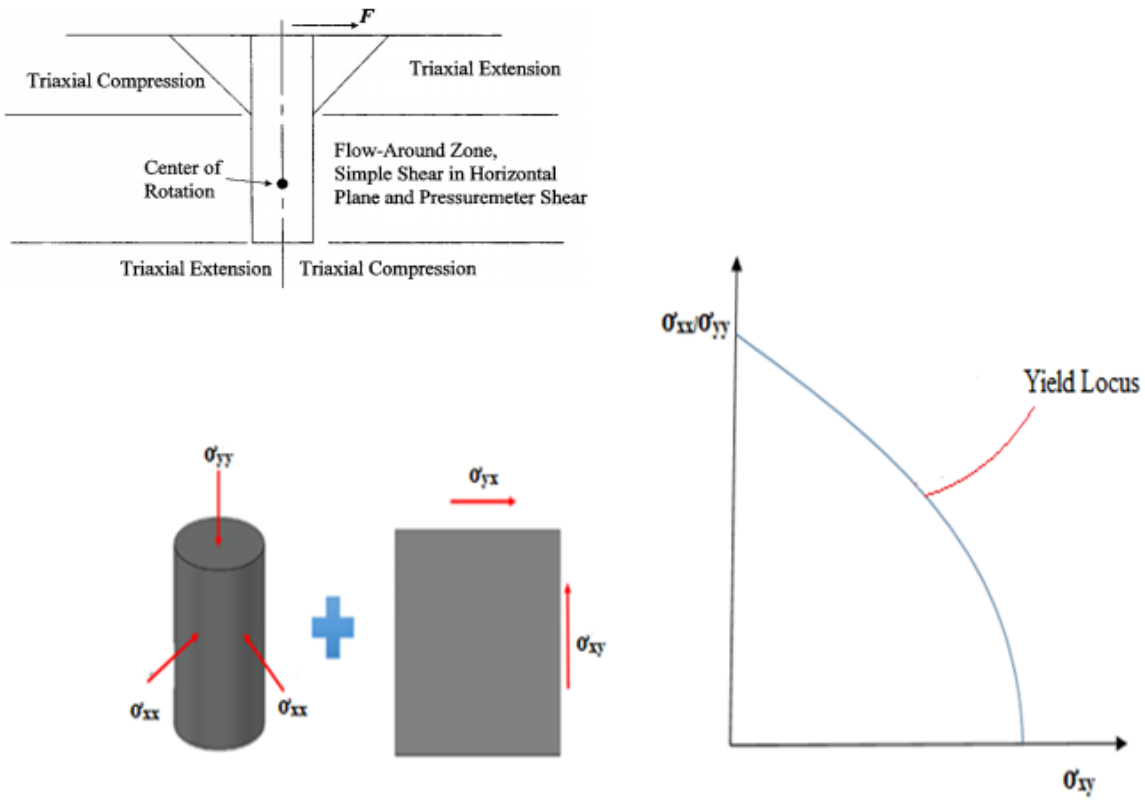

Figure 2. 2: Soil stress state around a caisson. Schematic diagram of triaxial and simple shear state, and yield locus (Adapted from: Aubeny, Han et al. (2003))

After a certain limit of elastic strain, corresponding to yield point, the material starts to experience plastic strains. Which means that if the material is unloaded it will not recover its original shape, rather a part (plastic) of total strain will become permanent feature of the material shape. The law which governs the plastic deformation of materials is known as yielding criteria.

Soil under a foundation undergoes different shearing modes as shown in Figure 2.2. As can be seen, some portion of soil is subjected to compression and extension which the yield criteria could be determined by corresponding triaxial test. But there is a portion of soil, which is subjected to combined loading. The yield criteria for this type of loading

case is represented by two dimensional curve also known as *yield locus*, which is function of certain stress components.

The yield locus remains fixed or expands or contracts depending on if the material shows perfectly plastic or strain hardening or strain softening behavior, respectively. Mostly commonly used yield loci are defined by von Mises and Tresca yield criteria.

Consider the application of stresses as shown in Figure 2.2. von Mises criteria is based on the concept that yielding occurs when:

$$J_2 = k^2 \tag{2.1}$$

Where;

J_2= second invariant of stress tensor

k= yield stress from simple shear test

It is known that magnitude of yield shear stress is equal to $(1/\sqrt{3})$ times of the tensile stress. That is;

$$k = \frac{\sigma_y}{\sqrt{3}} \tag{2.2}$$

Equating von Mises criteria (eq. 2.1) with shear yield strength (eq. 2.2), von Mises criteria can be written as:

$$\sigma_y = \sqrt{3J_2} \tag{2.3}$$

or

$$\sigma_y{}^2 = 3J_2 = 3k^2 \tag{2.4}$$

Substituting J_2 with Cauchy stress tensor

$$\sigma_y{}^2 = \frac{1}{2}[(\sigma_{11} - \sigma_{22})^2 + (\sigma_{22} - \sigma_{33})^2 + (\sigma_{33} - \sigma_{11})^2 + 6(\sigma_{23}^2 + \sigma_{31}^2 + \sigma_{12}^2) \quad (2.5)$$

or, in the the form of principal stresses

$$\sigma_y^2 = \frac{1}{2}[(\sigma_1 - \sigma_2)^2 + (\sigma_2 - \sigma_3)^2 + (\sigma_3 - \sigma_1)^2] \quad (2.6)$$

If stresses are uniaxial, then the yieding is shown by a nonlinear line. For 2D and 3D stress syetem, yield surafce is plotted as circle.

Henri Tresca, on other hand, expressed yield criteria as:

$$\sigma_y = \frac{1}{2}\max(|\sigma_{1-}\sigma_2|, |\sigma_{2-}\sigma_3|, |\sigma_{3-}\sigma_1|) \quad (2.7)$$

Figure 2.3 shows the comparison of von Mised and Tresca yield surfaces. von Mises yield locus is represented by circle while yield locus determined by Tresca is shown by hexagon. As can be seen for uniaxial or biaxial loading, the the strength by both the crietia is same. But for all other other loading conditions, von Mises estimates higher strength values than Tresca. The maximum difference in the values is shown for the case of pure shear.

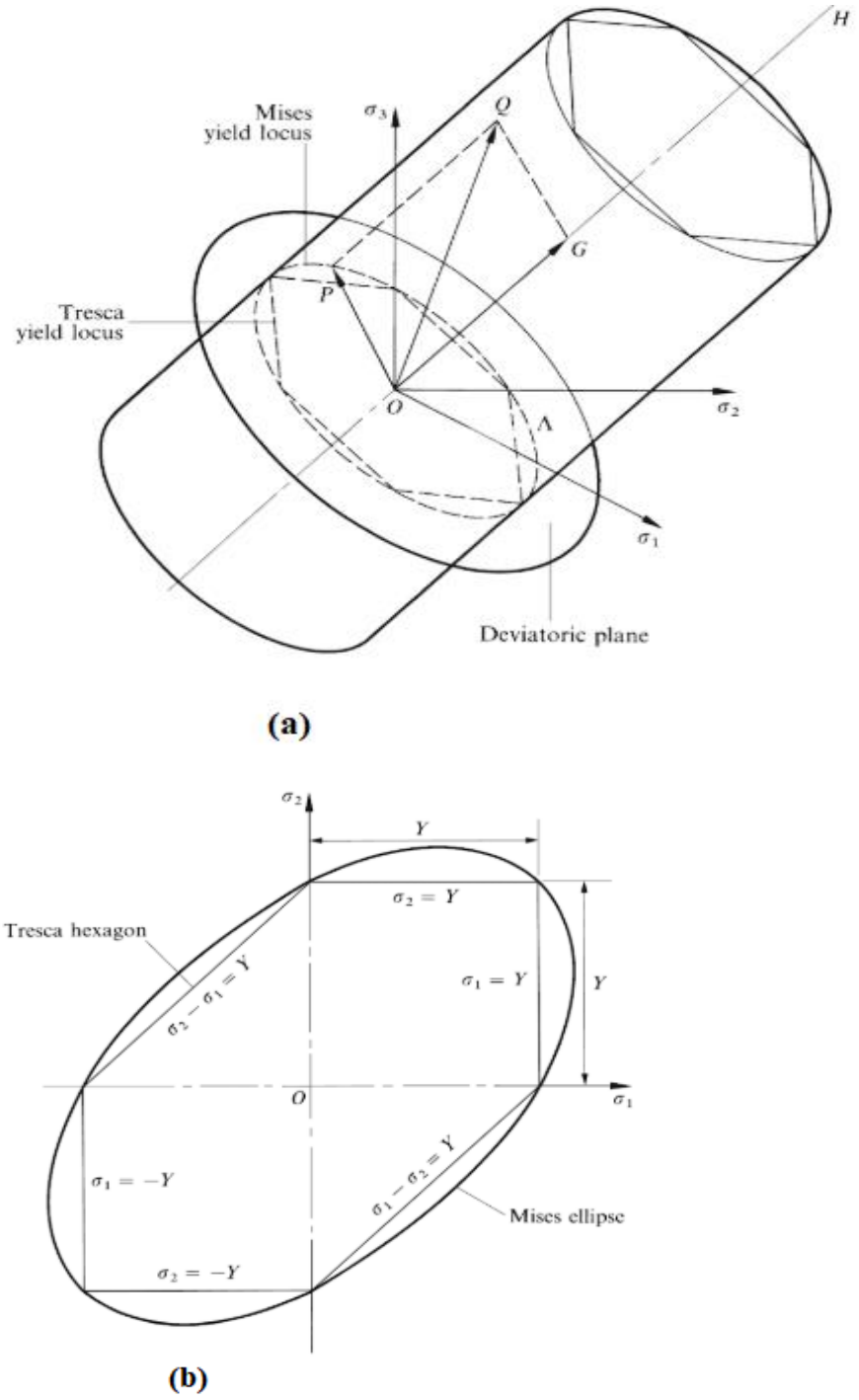

Figure 2. 3: Geometrical depiction of von Mises and Tresca yield criteria in principal stress space (a) 3D stress system (b) 2D stress system (Reprinted from: Chakrabarty, (2012))

2.4 Flow Rule

Flow rule defines the non-recoverable component of the total strain. When stress conditions in an element reach yield locus, any further application of load causes permanent strain in the material. Flow rule relates the plastic strain increment ($d\varepsilon^p{}_{ij}$) with deviatoric stress tensor increment ($\partial\sigma_{ij}$) by assuming that normal to yield surface and plastic strain increment has same direction.

Mathematically,

$$d\varepsilon_{ij}^{p} = \frac{\partial g}{\partial \sigma_{ij}} d\lambda \tag{2.8}$$

Where,

g = plastic strain potential function

$d\lambda$ = positive scalar, dependent on stress increment

Representing yield function by f, associated flow rule assumes that yield function f and plastic potential function g are same. This assumption is made for the simplicity, although many materials fall under non-associated flow rule. Under the associated flow rule, total strain can be resolved into elastic and plastic strain components so that plastic strain increment is normal to yield surface. Figure 2.4 shows the determination of plastic strain using associated flow rule.

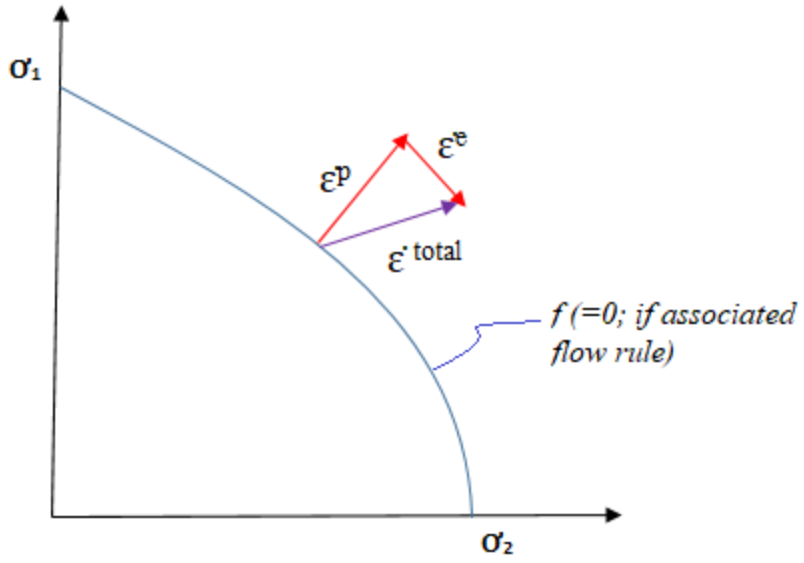

Figure 2. 4: Illustration of flow rule to determine plastic strain

2.5 Bound Theorems

In plasticity, two approaches are employed to estimate the ultimate load. One is based on equilibrium of stresses with the applied loads, which provides ultimate load always lower than actual load, hence called lower bound. Whereas, the other approach makes use of displacement or velocity field to determine collapse load which is always higher than actual load, hence upper bound. Following are the formal definition of lower bound and upper bound theorems:

2.5.1 Lower Bound Theorem

If the stress produced in a soil is in equilibrium internally at every point and equilibriums the externally applied loads while the remaining within elastic yield criteria, then the soil will carry loads safely, which means that estimated collapse load is guaranteed

to be on the lower side of actual collapse load. Lower bound theorem always provides the conservative estimate of collapse load.

2.5.2 Upper Bound Theorem

According to upper bound theorem, failure will occur due to external loads if for an anticipated failure mechanism, the rate of work done due to external loads is greater than the internal energy dissipation in the soil mass. The load estimated is unsafe for the soil mass since it is guaranteed to be higher than actual collapse load. The equation which are obtained by this theorem as known as work equation.

In soil, upper bound theorem is desirable since collapse mechanism can be defined in terms of internal energy dissipation rate and soil strength properties can be incorporated in the rate easily. To solution based on this theorem involves following steps:

1. A collapse mechanism should be assumed which should be valid and satisfying boundary conditions.
2. The dissipation of energy by external applied loads, including soil self-weight, due to small changes in displacement (or velocity) based on assumed collapse mechanism should be calculated.
3. A work equation is established for the assumed mechanism and the upper bound load is determined.
4. The solution should be refined by optimizing the parameters which define geometry of the assumed mechanism to calculate the least upper bound load, which is the final solution.

A mechanism is termed as valid if small changes (in displacement or velocity) happening due to assumed mechanism are compatible and kinematically admissible, which means that the failure mechanism should be continuous i.e. no overlapping or gapping should occur in the body and the direction which comes from the assumed failure mechanism should be able to define yield stresses which are used in the dissipation rate.

2.6 Energy Dissipation Rate

As discussed in the preceding section, calculation of energy dissipation rate is one of the building block of upper bound analysis. Soil failure is divided into two types while calculating energy dissipation rate calculation:

1. Energy dissipation in continuously deforming soil region
2. Energy dissipation rate in slip surfaces

Mathematical form of both the rates is constructed in following sections.

2.6.1 Energy Dissipation Rate in Continuously Deforming Soil Regions

Consider an element of soil as shown in Figure 2.5. The element is subjected to normal stresses σ_{xx} and σ_{yy} and shear stresses τ_{xy} and τ_{xy}. As the maximum shear stresses approach maximum undrained shear strength of soil s_u, the stress state will be on yield surface. Mathematically;

$$f = \left[\frac{(\sigma_{xx}-\sigma_{yy})^2}{4} + \frac{1}{2}(\tau_{xy}^2 + \tau_{yx}^2)^2\right]^2 - s_u = 0 \qquad (2.9)$$

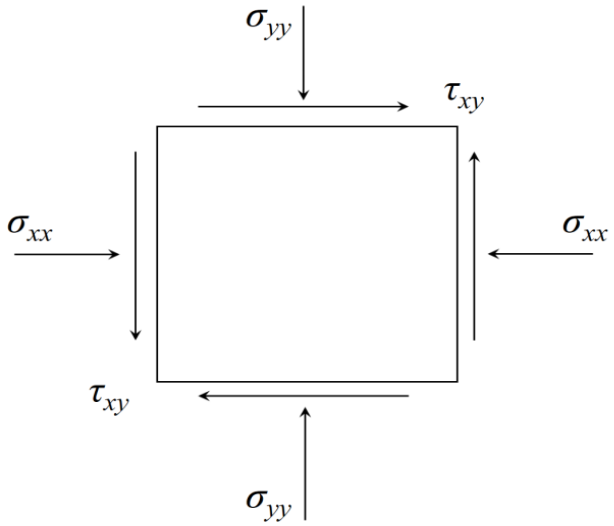

Figure 2. 5: A soil element under normal and shear stresses

For a 2D case, assuming the associated flow rule, plastic strains can be expressed as:

$$\dot{\varepsilon}_{xx} = \lambda \frac{\partial f}{\partial \sigma_{xx}} = \frac{1}{2}\lambda \left[\frac{(\sigma_{xx} - \sigma_{yy})^2}{4} + \frac{1}{2}\tau_{xy}^2 + \frac{1}{2}\tau_{yx}^2 \right]^{-1/2} \cdot \frac{2(\sigma_{xx} - \sigma_{yy})}{4} \tag{2.10}$$

$$\dot{\varepsilon}_{yy} = \lambda \frac{\partial f}{\partial \sigma_{yy}} = \frac{1}{2}\lambda \left[\frac{(\sigma_{xx} - \sigma_{yy})^2}{4} + \frac{1}{2}\tau_{xy}^2 + \frac{1}{2}\tau_{yx}^2 \right]^{-1/2} \cdot \frac{2(\sigma_{yy} - \sigma_{xx})}{4} \tag{2.11}$$

$$\dot{\varepsilon}_{xy} = \lambda \frac{\partial f}{\partial \tau_{xy}} = \frac{1}{2}\lambda \left[\frac{(\sigma_{xx} - \sigma_{yy})^2}{4} + \frac{1}{2}\tau_{xy}^2 + \frac{1}{2}\tau_{yx}^2 \right]^{-1/2} \tau_{xy} \tag{2.12}$$

Where λ is a scalar constant which depends on the magnitude of plastic strain.

For a purely incompressible material, the strain rate can be written as:

$$\dot{\varepsilon}_v = \dot{\varepsilon}_{xx} + \dot{\varepsilon}_{yy} = \frac{\partial \dot{u}}{\partial x} + \frac{\partial \dot{v}}{\partial y} = 0 \tag{2.13}$$

And the energy dissipation rate can be calculated using:

$$\dot{D} = \sigma_{ij}\dot{\varepsilon}_{ij}^{P} \tag{2.14}$$

Where σ_{ij} is a stress tensor and $\dot{\varepsilon}_{ij}^{P}$ is a tensor indicating plastic strain rate. Introducing the associated flow rule, plastic strain rate can be written as:

$$\dot{\varepsilon}_{ij}^{P} = \lambda \frac{\partial f}{\partial \sigma_{ij}} \tag{2.15}$$

Using equation 2.15 in 2.14, energy dissipation rate becomes

$$\dot{D} = \lambda \sigma_{ij} \frac{\partial f}{\partial \sigma_{ij}} \tag{2.16}$$

Using the equation 2.9 through 2.12, dissipation rate can be finally reduced to:

Combining equation 2.9 and equations 2.10, 2.11, and 2.12, the scalar λ can be written as:

$$\dot{D} = \frac{\lambda}{s_u} s_u^2 = \lambda s_u \tag{2.17}$$

$$\lambda = (2\varepsilon\square_{xx}^2 + 2\varepsilon\square_{yy}^2)^{1/2}$$

(2.18)

The final expression to calculate the energy dissipation rate is

$$\dot{D} = 2s_u \left(\dot{\varepsilon}_{xx}^2 + \dot{\varepsilon}_{xy}^2\right)^{1/2} \tag{2.19}$$

The above expression is for 2D mechanism. For a 3D mechanism, like the one which is assumed in laterally loads piles, dissipation rate for both von Mises and Tresca criteria can be determined respectively by:

$$\dot{D} = s_u \left(2\dot{\varepsilon}_{ij}^{P}\dot{\varepsilon}_{ij}^{P}\right)^{1/2} \tag{2.20}$$

$$\dot{D} = 2s_u \left|\dot{\varepsilon}^{P}\right|_{\max} \tag{2.21}$$

2.6.2 Energy Dissipation Rate along Slip Surface

To derive an expression of energy dissipation along slip surface consider a deformable block between two rigid blocks as shown in Figure 2.6. The deformable region has thickness *t* and unit width. The rigid block on the top of deformable region is moving

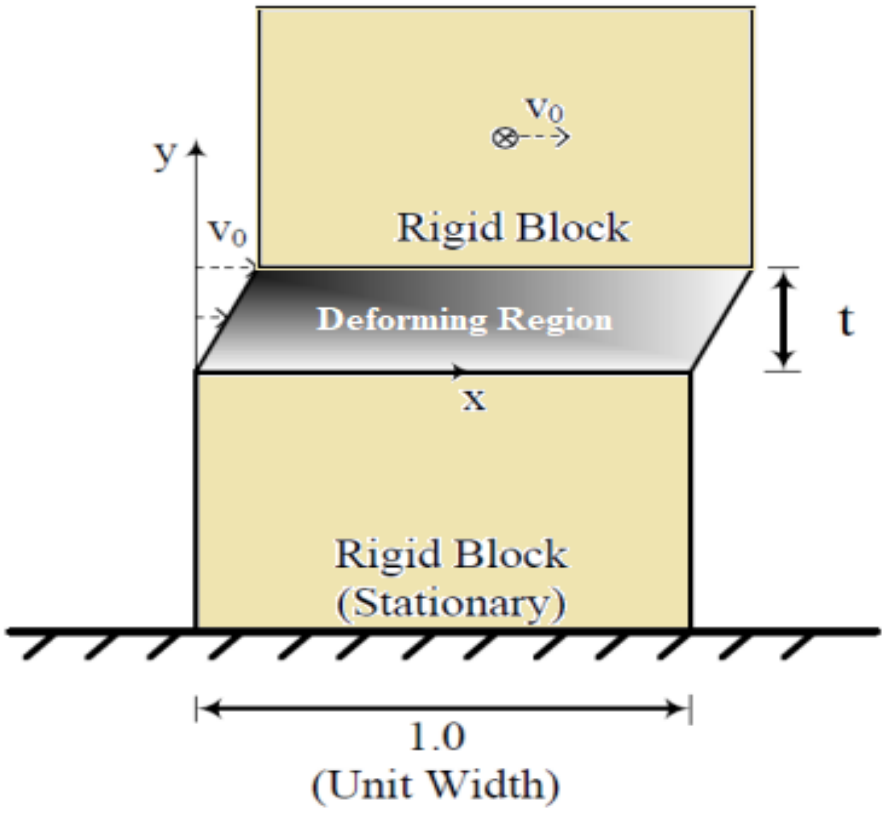

Figure 2. 6: A deformable region sandwiched between two rigid blocks

with a central velocity v_0 in horizontal direction. The velocity fields of deforming region are:

$$v_x = (v_0/t).\, y \qquad v_y = 0 \qquad v_z = 0 \tag{2.22}$$

The non-zero plastic strain components are $\dot{\varepsilon}_{xy}$ and $\dot{\varepsilon}_{yx}$ and are calculated by:

$$\dot{\varepsilon}_{xy} = \dot{\varepsilon}_{yx} = \frac{1}{2}\left(\frac{\partial v_x}{\partial y} + \frac{\partial v_y}{\partial x}\right) = \frac{v_0}{2t} \tag{2.23}$$

The von Mises yield criteria render energy dissipation along slip surface per unit volume

$$\dot{D} = 2s_u\left[\left(\frac{1}{2}\frac{v_0}{t}\right)^2\right]^{1/2} = s_u\frac{v_0}{t} \tag{2.24}$$

as:

The total energy can be calculated by integrating the energy rate over the entire volume. Using the thickness and width as 1, the total energy rate is

The energy dissipation rate expressions are used commonly in Murff-Hamilton method of analysis.

$$\dot{D}_{Total} = \int_V \dot{D}dV = \dot{D}\cdot V = s_u\frac{v_0}{t}(1\cdot t) = s_u v_0 \tag{2.25}$$

2.7 Plastic Limit Analysis

Plastic limit analysis can be explained by a stress strain curve for a soil under a footing, as shown in Figure 2.7. The curve shows an elastic behavior, a region of transition from elastic purely plastic region, a pure plastic region where material undergoes large strain with a very small increase in load, and a work hardening region and/or transformation of surface footing to sub-surface footing.

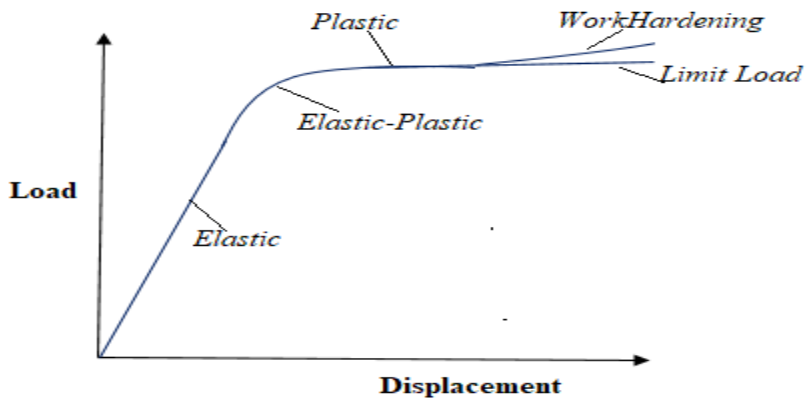

Figure 2. 7: Collapse load by plastic limit analysis

The curve doesn't define the collapse load itself, rather the collapse load is obtained corresponding to large deformations. Assuming the soil as perfectly plastic after elastic region and neglecting the work hardening zone leads to displacement without limit while the load remains constant. The load estimated based on this idealization is known as plastic limit load and provides a good approximation of actual collapse loads. This method of analysis is termed as Plastic Limit Analysis.

2.8 Analysis of Laterally Loaded piles

The ultimate lateral capacity of laterally loaded piles was first discussed by Broms (1964). The ultimate resistance (ΔH) was introduced as horizontal force (P) acting on the area composed by unite depth (Δz) and diameter of pile (D). Mathematically,

$$\Delta H = PD\Delta z \tag{2.26}$$

Whereas, for pure cohesive soil, the horizontal force can be related to undrained shear strength S_u by using a dimensionless bearing factor N_{ps} by:

$$P = N_p s_u \quad (2.27)$$

The above empirical factor N_{ps} was used by many researchers for the analysis of ultimate lateral capacity piles and caissons.

For purely horizontal pile movement Randolph & Houlsby (1984) presented a method of analysis using the plasticity theory. They considered a long cylinder translating in an infinite cohesive soil.

Matlock (1970) provided a detail investigation of capacity of laterally loaded piles by performing field as well as laboratory experiments. An analytical solution, inferring from the experimental results, was also proposed. Bang et al. (2011) performed the same investigation but on cohesion-less soil.

Murff & Hamilton (1993) proposed a method to find ultimate laterally capacity of piles in undrained conditions using upper-bound plastic limit analysis (PLA). Based on that they further concluded the unit lateral capacity of piles along the length. Since the upper bound method requires a failure mechanism and optimization of the parameters associated with the failure mechanism, they also proposed a simplified yet empirical unit lateral resistance factors *Np* as an alternate to upper bound PLA. Aubeny et al., (2001) made use of an empirical factor proposed by Murff & Hamilton (1993) and suggested a simplified method for undrained lateral capacity of piles. Both of the methods are discussed in detail in following sections.

2.8.1 Murff-Hamilton PLA for Laterally Loaded Piles

The first step towards upper bound PLA is to define a collapse mechanism. Based on experimental evidence, Murff & Hamilton (1993) assume a three-dimensional failure mechanism for laterally loaded piles as shown qualitatively in Figure 2.8. The collapse mechanism consists of three regions: (1) a conical failure wedge near the surface, (2) a plain strain zone assuming soil flowing around the pile, and (3) a hemispherical slip surface at pile tip; if relatively shorter pile or a plastic hinge in pile; if longer.

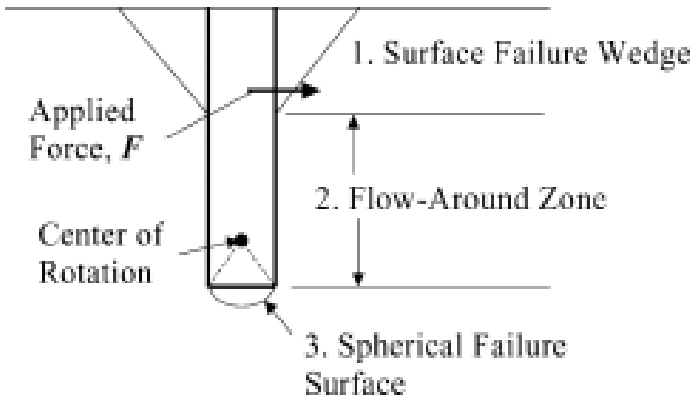

Figure 2. 8: Failure mechanism proposed by Murff and Hamilton (Reprinted from: Murff & Hamilton (1993))

The second step is to evaluate energy dissipation rate in the suggested collapse mechanism using relationship between yield criteria (von Mises or Tresca) and kinematically admissible velocity field for both the wedge and hemispherical slip surface. Whereas, for energy dissipation in flow around zone, Randolph & Houlsby (1984) methodology is applied.

The failure mechanism does not strictly satisfy the upper-bound criteria since, in transition from wedge to flow around zone, compatibility is not fully imposed and the plain

strain condition in flow around zone is not applicable except for translating piles. However, the formulation has been validated by experiments and numerical approximations and is confidently practiced in the industry. Salient features of Murff-Hamilton PLA are as follows (Aubeny & Murff, 2005):

1. A rotation point at depth *L0* is assumed for rotating pile whereas; for translation an infinite *L0* (or a large number if numerical model) is assumed.
2. The failure mechanism is defined using four optimization parameters: (1) depth of rotating point of caisson, (2) depth of near surface wedge, (3) radial extent of wedge at mudline, and (4) radial velocity variation in the wedge.
3. Model can accommodate plastic hinge formation for slender piles and a slip surface at the end of short pile.
4. The formulation has capability to incorporate soil anisotropy, soil pile adhesion, and gap formation behind the pile.

The energy dissipation and external work expressions for the PLA are discussed in detailed below (Murff & Hamilton, 1993).

2.8.1.1 Energy Dissipation Rate in the Wedge

Based on the collapse mechanism shown in Figure 2.6, the radial velocity in the wedge is expressed as

$$v_r = v_0 \left(\frac{R}{r}\right)^{\alpha} \left(1 - \frac{cz}{z_0}\right) \cos\theta \qquad (2.28)$$

Where $v0$ = virtual velocity at the top of pile, R = pile radius, z_0 = depth of wedge, c, α = optimization constants, r, z, θ = coordinates.

Since the purely cohesive soil is incompressible,

$$\dot{\varepsilon}_{rr} + \dot{\varepsilon}_{\theta\theta} + \dot{\varepsilon}_{zz} = 0 \tag{2.29}$$

Or alternatively, using the relationship between strain rate and velocity

$$\frac{\partial v_r}{\partial r} + \frac{v_r}{r} + \frac{\partial v_z}{\partial z} = 0 \tag{2.30}$$

Using (2.28) into (2.30)

$$v_z = g(r, \theta)\left(z - \frac{cz^2}{2z_0}\right) + h(r, \theta) \tag{2.31}$$

Where $h(r, \theta)$ = function dependent upon boundary conditions at the wedge and rigid soil considering velocity parallel to slip surface

$$\frac{v_r}{v_z} = -\frac{(r_0 - R)}{z_0} \tag{2.32}$$

on the slip surface which is defined by

$$z = z_0\left(\frac{r_0 - r}{r_0 - R}\right) \tag{2.33}$$

and

$$g(r, \theta) = v_0 \frac{(\alpha - 1)R^{\alpha}}{r^{1+\alpha}} \cos\theta \tag{2.34}$$

using equations (2.28), (2.31), and (2.32)

$$h(r, \theta) = v_0 z_0 \cos\theta \left(\frac{R}{r}\right)^{\alpha}\left(\frac{r_0 - r}{r_0 - R}\right)\left\{-\frac{1}{r_0 - r} + \left(\frac{c}{r_0 - R}\right) + \frac{1 - \alpha}{r}\left[1 - \frac{c}{2}\left(\frac{r_0 - r}{r_0 - R}\right)\right]\right\} \tag{2.35}$$

Using the energy dissipation expressions by von Mises and Tresca, respectively as:

$$\dot{E}_1 = s_u\sqrt{2\dot{\varepsilon}_{ij}\dot{\varepsilon}_{ij}} \tag{2.36}$$

$$\dot{E}_1 = 2s_u|\dot{\varepsilon}|_{\max} \tag{2.37}$$

the total energy dissipation in the wedge is

$$\dot{D}_1 = 2\int_{r=R}^{r=r_0}\int_{z=0}^{z=z_0[(r_0-r)/(r_0-R)]}\int_{\theta=0}^{\theta=(\pi/2)} \dot{E}_1 r\, d\theta\, dz\, dr \tag{2.38}$$

2.8.1.2 Energy Dissipation Rate at Wedge-Rigid Soil Interface

To determine the energy dissipation at the wedge-rigid soil interface, the tangential velocity is expressed as

$$|v_t| = \sqrt{v_r^2 + v_z^2} = v_r\sqrt{1 + \left(\frac{-z_0}{r_0 - R}\right)^2} \tag{2.39}$$

Using

$$r = -\frac{z}{z_0}(r_0 - R) + r_0 \tag{2.40}$$

v_r can be determined using equation (2.28)

and unit dissipation rate at slip surface is

$$\dot{E}_2 = s_u|v_t| \tag{2.41}$$

The total energy dissipation along the surface is

$$\dot{D}_2 = 2v_0\sqrt{1 + \left(\frac{z_0}{r_0 - R}\right)^2}\sqrt{1 + \left(\frac{R - r_0}{z_0}\right)^2}\cdot\int_0^{z_0} s_u \frac{R^\alpha\left(1 - c\frac{z}{z_0}\right)}{\left[r_0 - \frac{z}{z_0}(r_0 - R)\right]^{\alpha-1}}\, dz \tag{2.42}$$

2.8.1.3 Energy Dissipation Rate due to Soil-Pile Adhesion

One of the features of Murff-Hamilton analysis is that it can incorporate soil-pile adhesion. Energy dissipation rate is calculated if the soil around the pile is completely or partially adheres with be pile, by

$$\dot{E}_3 = \eta s_u|v_t| \tag{2.43}$$

Where η is called adhesion factor and taken 0 for no adhesion and 1 for full adhesion. The velocity v_t is determined as resultant of vertical and circumferential velocity as

$$v_t = \sqrt{v_z^2 + v_c^2} \tag{2.44}$$

$$v_c = v_0 \sin \theta \tag{2.45}$$

v_z is determined using equations (2.31), (2.34), and (2.35), whereas v_c is calculated by

Total energy dissipation rate due to soil-pile adhesion is

$$\dot{D}_3 = 2 \int_{z=0}^{z=z_0} \int_{\theta=0}^{\theta=(\pi/2)} \eta s_u \sqrt{v_z^2 + v_c^2}\, R\, d\theta\, dz \tag{2.46}$$

2.8.1.4 Energy Dissipation Rate below Wedge and Above Rotation Point

Soil below the soil wedge is assumed to be in plane-strain state. The unit dissipation rate along the pile length is

$$\dot{E}_4 = D \cdot s_u \cdot N_p \cdot v \tag{2.47}$$

Where Np is determined by Randolph-Houlsby solution for plane-strain condition. The total dissipation rate above the center of rotation and for $(z_0/c) \leq l$ is

$$D_4 = \int_{z'=0}^{z'=(z_0/c)-z_0} 2v_0 z' \left(\frac{c}{z_0}\right) s_u N_p R\, dz' \tag{2.48}$$

and for $(z_0/c) > l$

$$D_4 = \int_{z'=(z_0/c)-l}^{z'=(z_0/c)-z_0} 2v_0 z' \left(\frac{c}{z_0}\right) s_u N_p R\, dz' \tag{2.49}$$

2.8.1.5 Energy Dissipation Rate below Rotation Point

If $(z_0/c) < l$ then the total energy dissipation rate below the center of rotation along the pile length is

$$\dot{D}_5 = \int_0^{l-(z_0/c)} 2v_0 z' \left(\frac{c}{z_0}\right) s_u N_p R \, dz' \tag{2.50}$$

2.8.1.6 Energy Dissipation Rate due to Plastic Hinge Formation

If the work done in pile due to plastic moment at the center of rotation is less than the energy dissipation rate below the center of rotation then plastic hinge energy dissipation should be considered instead (i.e. pile plastic hinge is critical). The energy dissipation rate for that is

$$\dot{D}_5 = M_2\dot{\theta} = |M_2| \frac{v_0}{\left(\frac{z_0}{c}\right)} \tag{2.51}$$

2.8.1.7 Work Done by Wedge Soil in Gravitational Field

When the soil moves in the wedge, the work done is calculated using

$$\dot{W}_1 = 2 \int_{r=R}^{r=r_0} \int_{z=0}^{z=(r_0-r)/(r_0-R)} \int_{\theta=0}^{\theta=\pi/2} v_z \gamma' r \, d\theta \, dz \, dr \tag{2.52}$$

2.8.1.8 Energy Dissipation Rate along Slip Surface at Caisson Tip

As discussed earlier, for short stubby piles (e.g. caissons), pile end resistance has significant share in the total lateral capacity. Considering this fact, Murff & Hamilton (1993) assumed a hemi-spherical slip surface at pile end. The energy dissipation rate along the slip surface is

$$D_6 = \frac{v_0 R_2^3 c}{z_0} \int_{\phi=0}^{\phi=2\pi} \int_{\omega=0}^{\omega=\sin^{-1}(R/\sqrt{R_1^2+R^2})} s_u \sqrt{\cos^2\omega + \sin^2\omega \sin^2\phi} \sin\omega \, d\omega \, d\phi \tag{2.53}$$

Where

R_1 = distance between point of rotation and tip of pile

R_2= radius of Hemispherical slip surface, and expressed as

$$R_2 = \sqrt{R_1^2 + R_2^2} \tag{2.54}$$

ϕ = Angular coordinate with reference to the center line of the pile

ω = Angle about pile centerline

2.8.1.9 Empirical Unit Lateral Resistance Factor

Murff & Hamilton (1993) used the plastic limit formulation to predict an empirical dimensionless unit lateral resistance factor, N_{ps}, which is applicable for uniform and linearly varying shear strength profiles. Mathematically,

$$N_{ps} = N_1 - N_2 \exp(-\eta z/D) \tag{2.55}$$

For a mudline shear strength S_{u0} and increasing at a rate k per unit depth, η for a laterally load pile of diameter D is:

$$\eta = 0.25 + 0.05\rho \quad \text{for } \rho < 6$$
$$\eta = 0.55 \quad \text{for } \rho > 6 \tag{2.56}$$

where,

$$\rho = S_{u0}/kD \tag{2.57}$$

The parameter N_1 is unit lateral resistance factor away from mudline which Randolph& Houlsby (1984) proposed for infinitely long cylindrical piles as 9.42 and 11.94 for smooth and rough caissons, respectively. Whereas N_2 is determined form difference (N_1-N_2) which is 2.0 and 2.82 for smooth and rough caissons, respectively.

2.8.2 Simplified Method for Laterally Loaded Piles

Murff-Hamilton PLA requires considerable computational energy since it involves integration of volume and surface integrals for energy dissipation rate calculation. Furthermore, optimizing the geometry by associated parameters to reach a least upper bound solution is a complex task. Aubeny et al. (2003) formulated a simplified method of analysis by using the equation (2.55) and using the observation that N_{ps} is independent of depth of the center of the rotation of a pile (Figure 2.9). The formulation is limited to uniform or linearly varying shear strength profiles along the depth *z* of pile, that is:

$$S_u = S_{u0} + k.z \tag{2.58}$$

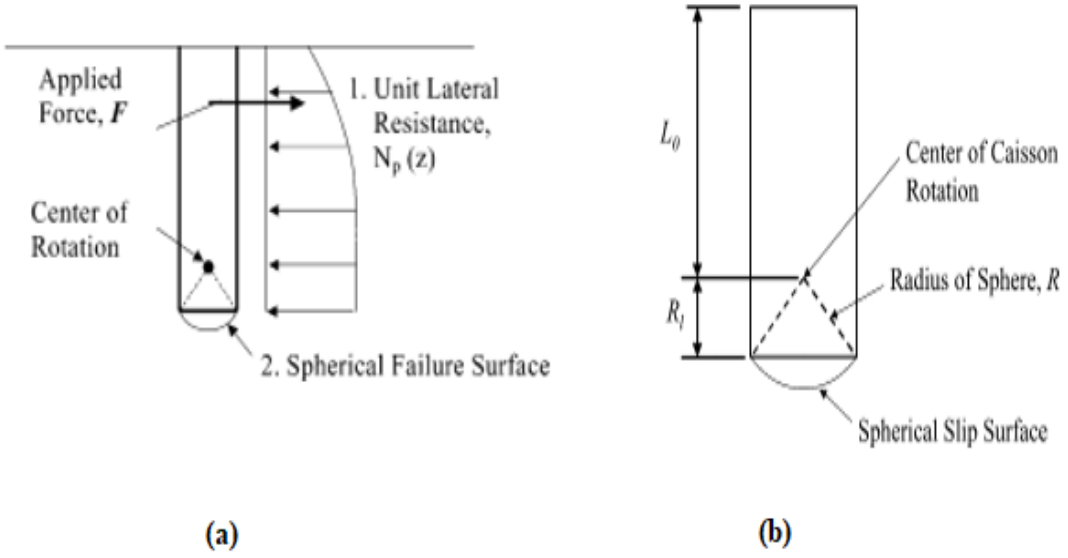

Figure 2. 9: Simplified analysis failure mechanism for (a) Side resistance (b) End resistance (Adapted from: Aubeny et al., (2001))

2.8.2.1 Energy Dissipation due to Side Resistance

Assuming a virtual angular velocity $\dot{\beta}$ about the center of rotation as shown in Figure 2.7, the velocity along the depth can be written as $v = (1-z/L_0)v_0$, where v_0 is velocity at free surface. The unit energy dissipation rate is expressed as:

$$d\dot{E} = N_p s_u \left| \left(1 - \frac{z}{L_o}\right) v_o \right| D dz \tag{2.59}$$

Where, D = Pile diameter; N_p is expressed as

$$N_p = N_1 - N_2 \exp(-\eta z/D) \tag{2.60}$$

For the case of full adhesion between behind the pile (weightless soil), the total energy dissipation rate for side resistance is:

$$\dot{D}_s = v_o D \int_0^{L_f} \left[\left(N_1 - N_2 \exp\left(-\frac{\xi z}{D}\right) \right) \left(s_{u0} + s_{u1} z\right) \left| 1 - \frac{z}{L_o} \right| \right] dz \tag{2.61}$$

Or, if the gap is formed behind the pile, then:

$$\dot{D}_s = v_o D \int_0^{L_f} \left| 1 - \frac{z}{L_o} \right| \left(N_p s_u + \gamma' z\right) dz \tag{2.62}$$

2.8.2.2 Energy Dissipation Due to End Resistance

A hemispherical failure mechanism about the center of rotation is assumed for end bearing resistance calculation. The energy dissipation rate at the end of the piles is:

$$\dot{D}_e = \frac{R_2^3 v_o}{L_o} \int_{\phi=0}^{2\pi} \int_{\omega=0}^{\sin^{-1}\left(1/\sqrt{(R_1/R)^2+1}\right)} \left\{ s_{u0} + \left(L_o + R_2 \sin\omega\right) s_{u1} \right\} \mathbf{x} \sqrt{(\sin\omega\sin\phi)^2 + (\cos\omega)^2} \sin\omega \, d\omega \, d\phi \tag{2.63}$$

Where R = radius of caisson, $R_1 = L_f - L_0$,

$R_2 = (R_1^2 + R^2)^{1/2}$ = Radius of hemispherical slip surface,

ϕ = angular coordinates about centerline of caisson in horizontal plane (0 to 2π), and

ω = angular coordinates about centerline of caisson (0 to $\sin^{-1}(R/R_2)$).

For translating caissons, the expression for energy dissipation rate is simply:

$$\dot{D}_{et} = v_o(s_{u0} + s_{u1}L_f)\frac{\pi D^2}{4} \tag{2.64}$$

3 CAPACITY OF CAISSONS IN BILINEAR SOIL STRENGTH PROFILES

3.1 Introduction

Soils in oceanic environment are very common to have layers of different shear strength along the depth. One of the most common ones is a soil system of two layers with each layer strength linearly varying with the depth. Murff & Hamilton (1993) provided a formulation to find the ultimate lateral capacity of piles by using the concept of plastic limit analysis (PLA). The method has been discussed in detail in Chapter 2. The major advantage of the approach is that it can incorporate complexities in soil strength profiles as described in Chapter 1. Moreover, the method can be transformed into a MATLAB code and optimization can be performed effectively. However, the optimization also becomes a drawback of the model in a sense that it requires a significant computational energy which is not available in industry all the time.

Based on these considerations, Aubeny et al., (2001) developed a simplified method of analysis which is valid for soils that have uniform or linearly increasing undrained shear strength. The reason the method, in current form, is not valid to complex strength profiles is because it makes use of the empirical lateral resistance factor N_{ps} which is dependent on mudline soil strength and the strength gradient at the same time. The factor N_{ps} was proposed by Murff & Hamilton (1993) using the results of upper bound PLA and is empirical in nature.

To enable the simplified method of analysis be valid for bilinear shear strength profile, an approach is needed which could transform the profile to its equivalent linearly

varying profile. The approach should be logical and hold true for variety of strength gradient combinations. The other alternative is to propose a modified dimensionless factor N_p that could embrace different strength profiles. Effect of variation of layers' thicknesses, and optimum load attachment depth are also needed to be studied. Since Murff-Hamilton analysis method has been proved to handle the complexities of soil, it can be used as standard to compare the results of any proposed approach. The words *pile* and *caisson* are used interchangeably in the text.

3.2 Procedure

The general analysis has been carried out for eight different caisson diameters as show in Table 3.1. Length to diameter ratio (aspect ratio, L_f/D) for each pile was varied from 2 to 8, which are typical of caissons. A first layer depth of 5 m was considered for all analysis except for caisson diameters of 1.83 m (72 in), 2.13 m (84 in), and 2.44 m (96 in) corresponding to aspect ratio 2, where a depth of 3 m was used. This anomaly was necessary to make sure that caisson extends well into the second layer. After the general analysis, parametric studies were made considering variation in first layer thickness, relative change in shear strength gradient, changing load attachment depth, and formation of gap behind the caisson. For parametric studies, an aspect ratio of 6 was selected, which is conservative selection so that effect of first layer on the analysis in the second layer (if any) could also be incorporated in ultimate lateral load calculation. Table 3.2 contains the variation of the data used for analyses.

Table 3. 1: Piles diameters selected

Pile No.	Diameter (in)	Diameter (m)
1	72	1.83
2	84	2.13
3	96	2.44
4	108	2.74
5	120	3.05
6	132	3.35
7	144	3.66
8	156	3.96

Table 3. 2: Variation of parameters for sensitivity analyses

L_f/D	k_1/k_2	x_1/L_f	L_i (Both Suction and No-suction)
2	0.2	0.2	0
3	0.3	0.3	$2/3L_f$
4	0.4	0.4	Pure Translation
5	0.5	0.5	
6	0.6	0.6	
7	0.7	0.7	
8	2	0.8	
	3		

The analysis was made on ultimate lateral capacity (P_u) and dimensionless unit resistance factor (N_{ps}). For N_{ps} analysis, the simplified lateral resistance factor was

$$N_p = \frac{\Delta F}{s_u D \Delta L} \qquad (3.1)$$

compared with the one calculated considering the small incremental depth in Murff-Hamilton analysis. i.e.

The whole procedure can be summarized in following steps:

1. Determination of procedure to transform bilinear strength profile into its equivalent one.
2. Introduction of the equivalent strength profile into Simplified Method of Analysis
3. Incorporation of the bilinear strength profile into Murff-Hamilton PLA.
4. Computation of lateral resistance by both Simplified Method and Murff-Hamilton PLA.
5. Analysis of results and parametric studies.

3.3 Bilinear Shear Strength Profiles

This study was carried out on clay and silt sediment undrained shear strengths for the Gulf of Maine. In terms of undrained shear strength, the soil can be categorized as Very Soft clay. Up to depth of 5 meters, geological epoch of soil is Holocene which can classified as MH, with a water content ranging 90% to 110%. Soil below 5 meters is Pleistocene, falling in classification of CH/CL and water content varying from 30% to 50%. Direct Simple Shear (DSS) strength was used as undrained shear strength in the analyses. Sea water unit weight of 10.1 KN/m^3 was used for soil parameters determination. Table 3.2 and 3.3 shows the soil shear strength for different shearing mode and other soil parameters. Figure 3.1 shows the plot of variation of undrained shear strength along depth considering different modes of shearing.

Table 3. 3: Gulf of Maine soil parameters

Depth, z	**Sediment**	γ_t	ω	e_0	**LL**	**PL**	**PI**	**LI**	c_{v0}
m		**kN/m^3**	**%**	**-**	**%**	**%**	**%**		**m^2/yr**
0 to 5	Holocene MH	14.3	100	2.7	94	51	43	1.1	5
> 5	Pleistocene CH/CL	17.4	40	1.08	42	25	17	0.9	10

Table 3. 4: Gulf of Maine undrained shear strength under different shearing modes

Depth z	**Sediment**	s'_{v0}	K_0	S_u**(DSS)**	S_u**(TC)**	S_u**(TE)**
m		**kPa**		**kPa**	**kPa**	**kPa**
0	N/A	0	-	1.4	2	1.1
0 to 5	Holocene MH	4.20z	0.65	1.4 + 0.92z	2.0 + 1.34z	1.1 + 0.76z
> 5	Pleistocene CH/CL	21.0+ 7.30(z – 5)	0.5	6.0 + 1.61(z – 5)	8.7 + 2.34(z – 5)	4.9 + 1.31(z – 5)

3.4 Transformation of Bilinear Strength Profile to Equivalent Linear

It is evident form the filed data, many soil strengths are complex than uniform or linearly varying profiles. To study the effect of these complexities, two categories of variations were made for this study: (1) change in thickness of first layer keeping the

gradient of first layer (k_1) and of second layer (k_2) constant, and (2) change in k_1/k_2 ratio while keeping the thickness of first layer constant.

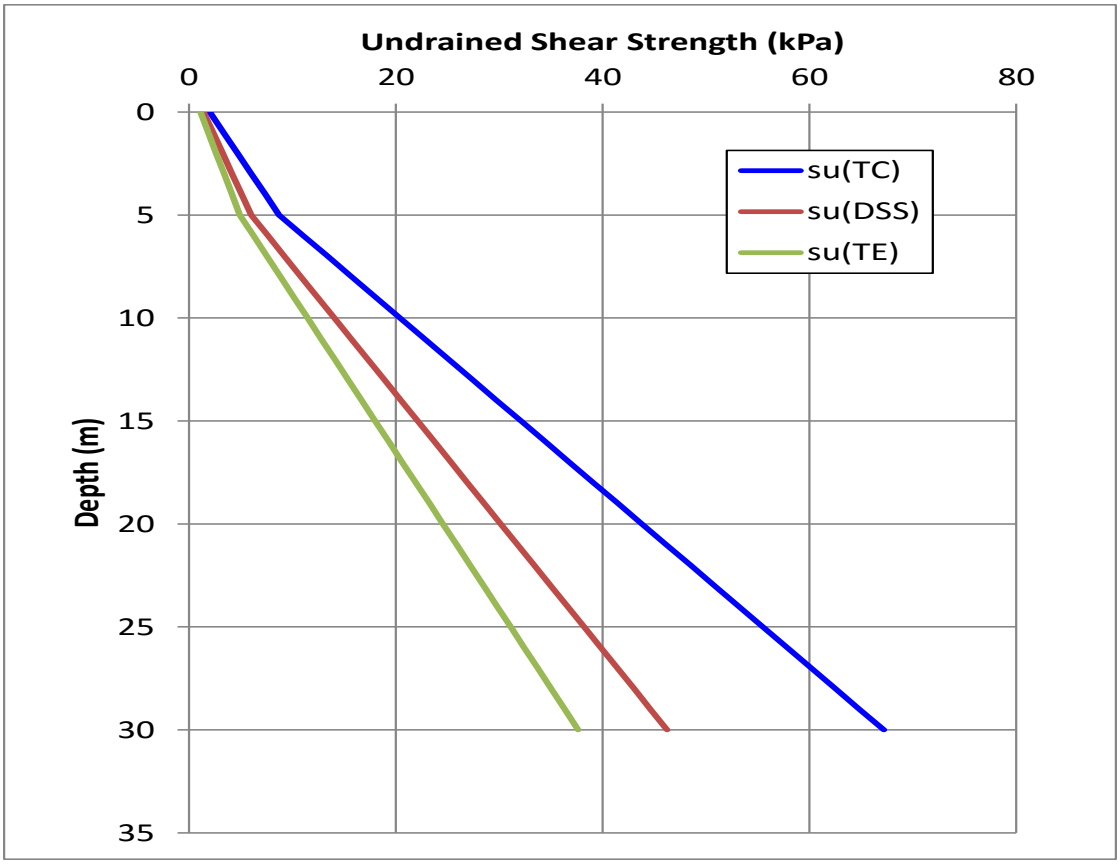

Figure 3. 1: Plot of undrained shear strengths under different shearing modes

Since the simplified analysis method can only be used for uniform or bilinear soil strengths, there was a need to change the two-layered soils of different strength gradients into an equivalent linear profile. To do this, a procedure was needed to be devised which could not only fulfill the requirement of the simplified analysis method but should also render results with an acceptable error. The basic principle followed here is that resultant of forces for both the profiles should be same. Moreover, since the simplified method uses the mud-line strength along with strength gradient, the same value for mud-line strength was assigned to the equivalent profile.

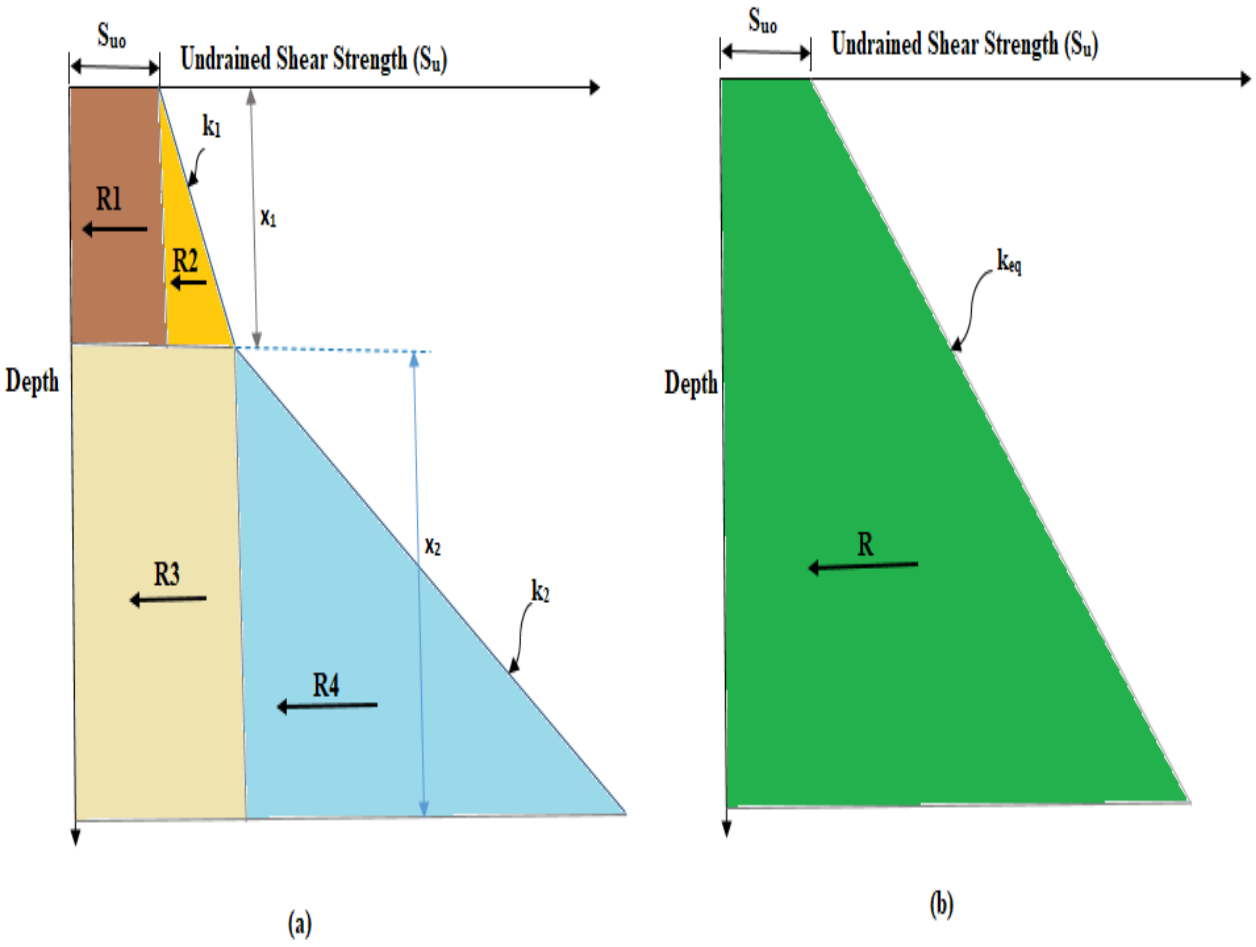

Figure 3. 2 Bilinear shear strength profile forces calculation

To calculate the resultant of forces offered by the soil, bilinear shear strength profile was divided into regular shapes (triangles and rectangles), as shown in Figure 3.2. The expressions for the calculations are as follows:

$$R_1 = S_{u0} * x_1 \tag{3.2}$$

$$R_2 = k_1 * \frac{1}{2} x_1^2 \tag{3.3}$$

$$R_3 = S_{u0} * x_2 \tag{3.4}$$

$$R_4 = k_2 * \frac{1}{2} x_2^2 \tag{3.5}$$

$$M_1 = R_1 * \frac{1}{2} x_1 \tag{3.6}$$

$$M_2 = R_2 * 2\frac{1}{3} x_1 \tag{3.7}$$

$$M_3 = R_3 * (x_1 + \frac{1}{2} x_2) \tag{3.8}$$

$$M_4 = R_4 * (x_1 + 2 * \frac{1}{3} x_2) \tag{3.9}$$

$$M_T = M_1 + M_2 + M_3 + M_4 \tag{3.10}$$

Whereas

$$R = R_1 + R_2 + R_3 + R_4 \tag{3.11}$$

$$\bar{x} = M_T / R \tag{3.12}$$

$$k_{eq} = \frac{2(R - S_{u0} * L_f)}{L_f^2} \tag{3.13}$$

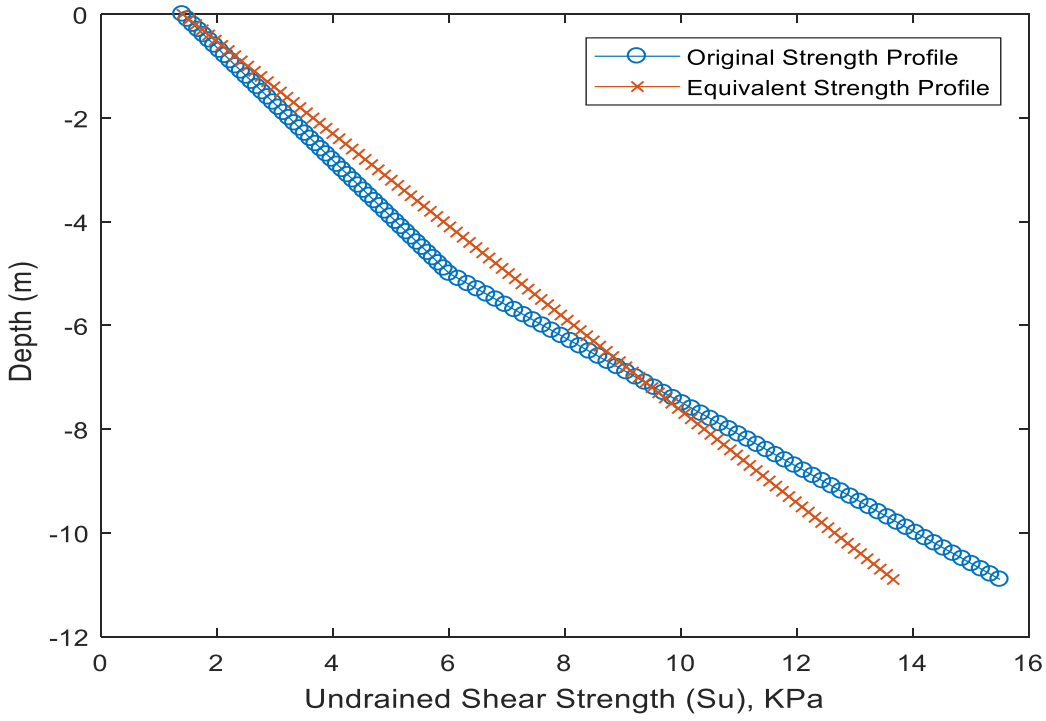

Figure 3.3: Plot of original bilinear and equivalent linear shear strength profile

Where, Lf = depth of caisson/pile,

R_1, R_2, R_3, R_4 are forces acting due to soil in each shape

M_1, M_2, M_3, M_4 are moments of the forces

A MATLAB subroutine was developed to change bilinear profile into equivalent linear profile (presented in APPENDIX A). A plot of original and resulted equivalent profile determined by MATLAB routine is shown in Figure 3.3.

3.5 Introduction of Equivalent Linear Profile into Simplified Analysis

Once the equivalent linear profile was obtained, next step was to introduce it into the MATLAB code for simplified analysis—a method proposed by Aubeny et al. (2001). The simplified method calculates the lateral capacity of suction caisson anchors by equating the external work rate to the internal dissipation rate, considering a generalized plastic limit analysis (detail in Chapter 2). The internal dissipation rate is computed in two steps:

First, it calculates the side resistance of caissons by integrating the unit energy dissipation rate at each point along the side of caisson. For that, the bearing factor (N_{ps}) is multiplied along with shear resistance (S_u), pile diameter (D) and virtual velocity (v_1) of soil along the caisson depth. i.e.

$$\dot{D}_s = \int (N_{ps} S_u D v_1) dz \qquad (3.8)$$

As discussed earlier, N_{ps} requires the soil profile to be uniform or linear due to its dependency on a function η which, in turn, depends on mudline strength and strength gradient at the same time. Therefore, equivalent shear strength gradient (k_{eq}), was used to determine N_{ps}. However, for undrained shear strength (S_u) at each point, original bilinear

profile was used. Hence, effect of difference of equivalent strength profile from bilinear strength profile is limited to N_{ps} calculation only.

Second, end bearing resistance is computed considering a hemispherical slip surface or simply the shear resistance of in-plane circular section for rotation or translation of pile, respectively. Again, the original S_u values corresponding to each point along the pile longitudinal axis were used for the energy dissipation rate calculations.

3.6 Incorporation of Bilinear Profile into Murff-Hamilton PLA

Murff-Hamilton method of analysis was used to compare the results obtained from the simplified analysis. The method determines the lateral capacity of caissons by computing the internal energy dissipation rate at rigid soil-wedge interface, with in the wedge, due to caisson-soil adhesion, in the soil below the wedge and above the rotation-point, in the soil below the point of rotation or, alternatively, work done by plastic moment around the point of rotation, work done by soil in the field of gravity, and the energy dissipation by the caisson tip. The method works on optimization principle and has a major advantage among the available analysis method that it can incorporate the complexities of the soil profiles (discussed in detail in Chapter 2).

The original Murff-Hamilton MATLAB code was modified to introduce the bilinear strength conditions. Each of the above dissipation rates or work done computation uses the soil shear strength, hence, modification in the code to accommodate the bilinear strength profile was repeated for each computation. One hundred optimizations were run to compute the ultimate lateral capacity.

3.7 Analyses

The following sections provide the comparison on the caisson analysis for both Simplified Analysis and Murff-Hamilton PLA. Initially, analysis was carried out by varying the aspect ratio (L_f/D), while keeping the layer thicknesses and gradient same. Later, to validate the proposed methodology of converting bilinear soil profile into equivalent linear, analyses were carried out under different combinations of layer thicknesses and strength gradients. Comparisons were also made considering the variation in load attachment depth and gapping behind the pile.

3.7.1 General Analysis

Figure 3.4 (a) through 3.4 (d) show the results of analyses by Murff-Hamilton PLA and Simplified Analysis for piles of diameter 1.83 m (72 in), 2.44 m (96 in), 3.05 m (120 in), and 3.66 m (144 in). The results for other piles from Table 3.1 are presented in APPENDIX B. The piles were considered to be in translation. For this analysis, the soil conditions provided in Table 3.3 were used. Complete suction (no gap) behind the pile was considered.

To present the comparison, ultimate lateral capacity (P_{ult}) was normalized with $5S_uDL$. For lower L_f/D ratio, e.g. 2, Murff-Hamilton analysis has slightly higher values than Simplified Analysis with maximum difference of 3.6% among all caissons diameters. However, for higher L_f/D ratios, the analyses yield very close results.

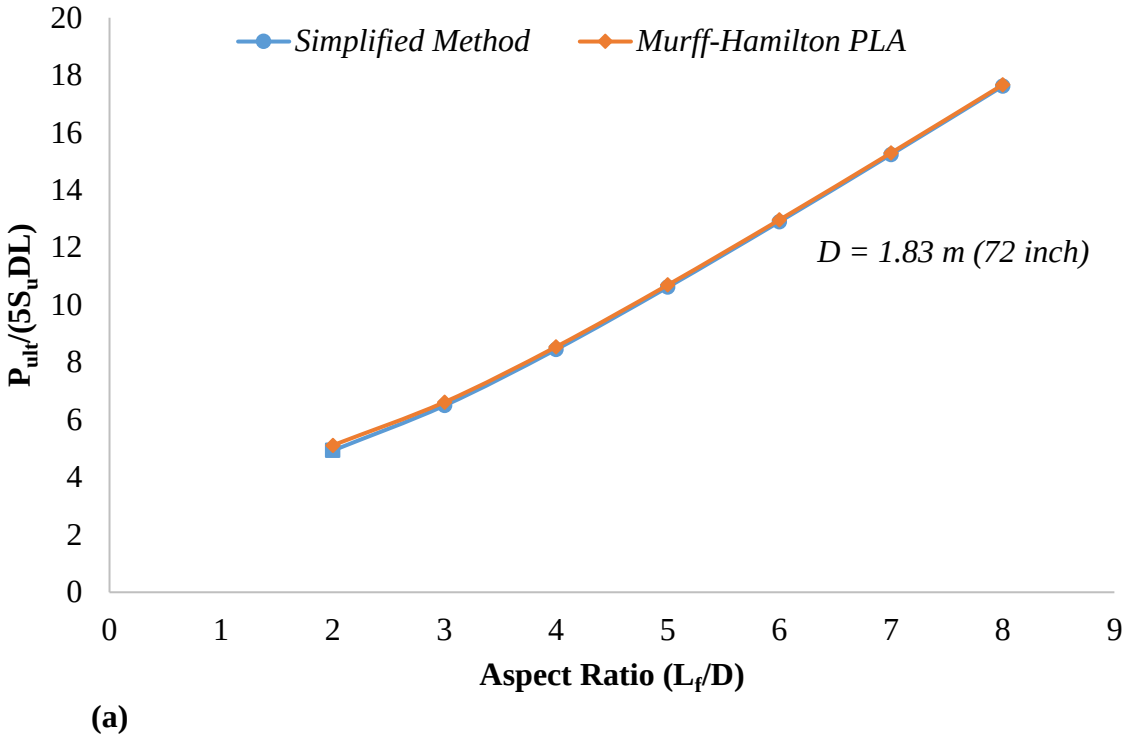

(a)

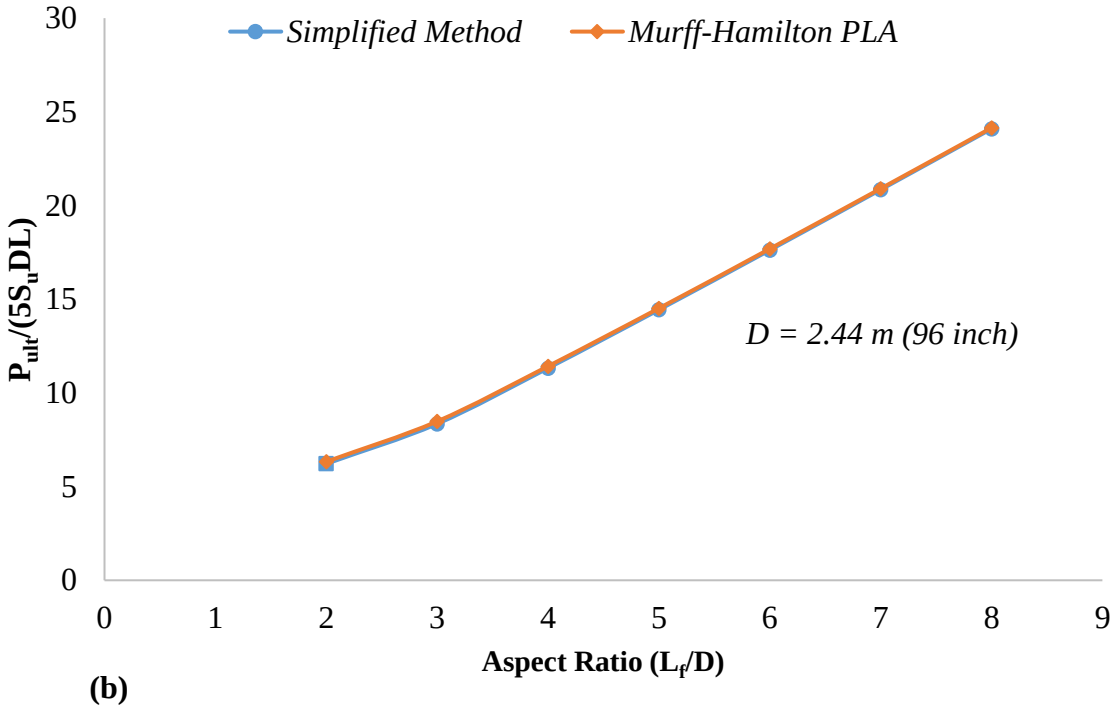

(b)

Figure 3.4: Normalized lateral capacity for different aspect ratios

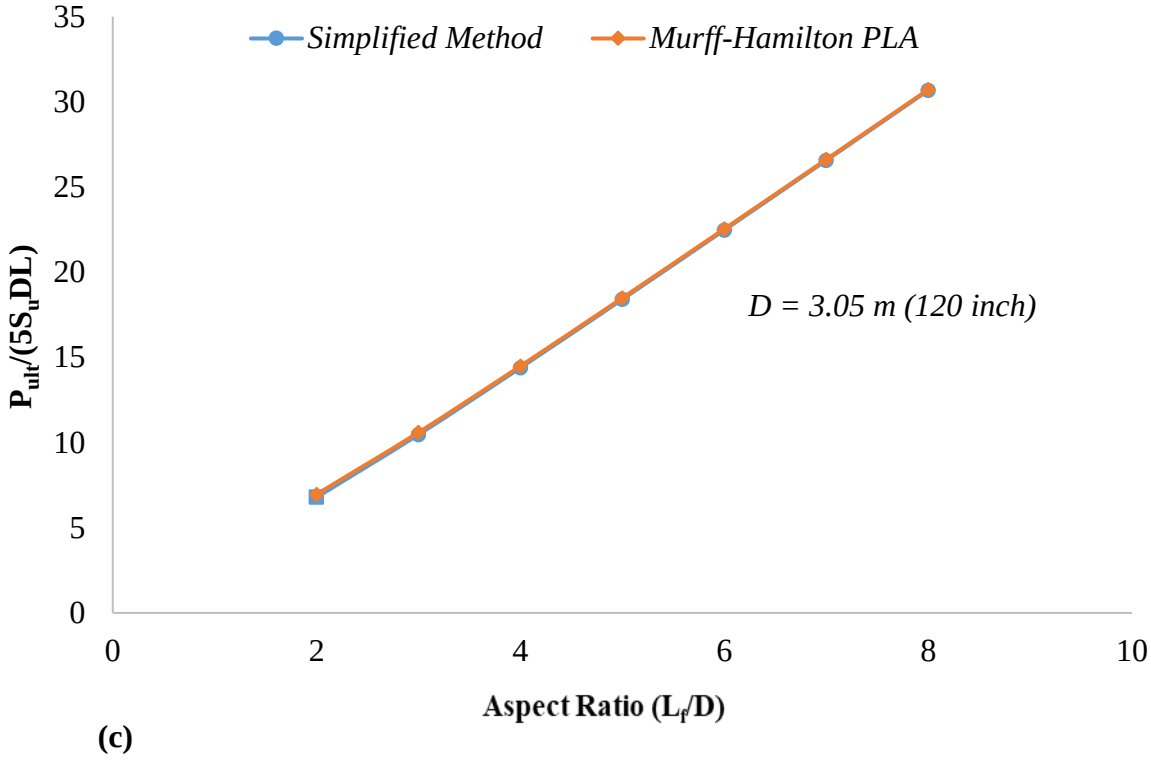

(c)

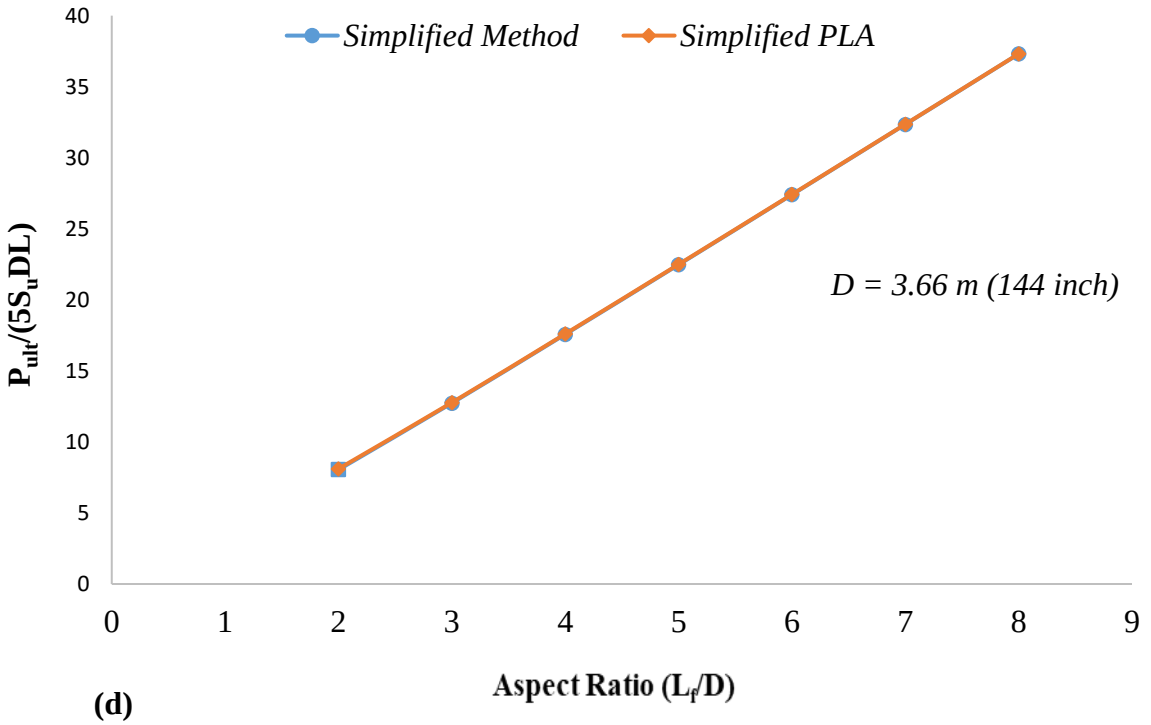

(d)

Figure 3.4 Continued.

It can be seen that as caisson diameter increases, the normalized capacities from both the methods match more closely.

3.7.2 Effect of Layer Thickness Variation on Ultimate Capacity

To study the comparison of ultimate capacity by Simplified Method and Murff-Hamilton PLA under different thicknesses of first layer, analysis was carried out by varying the first layer depth.

Seven depths were considered considering the first layer depth varying from 20% of total depth to 80%. Normalized ultimate lateral capacity of piles was plotted against the ratio of first layer thickness to total depth of caisson as shown in Figure 3.5. Results for piles of diameter 1.83 m (72 in), 2.44 m (96 in), 3.05 m (120 in), and 3.66 m (144 in) are presented here, whereas plots for other piles from Table 3.1 are presented in APPENDIX B. Fixed pile head that is; translating piles were assumed. No gapping behind the pile was considered during the analysis. As the aspect ratio for caissons varies typically from 2 to 8, an intermediate ratio of 6 was selected for all the analyses.

Since the gradient of first layer is relatively smaller than that of second layer, increase in thickness leads to lower ultimate capacity. The results from both Simplified Analysis and Murff-Hamilton PLA match very closely with each other, as shown by overlapping plots.

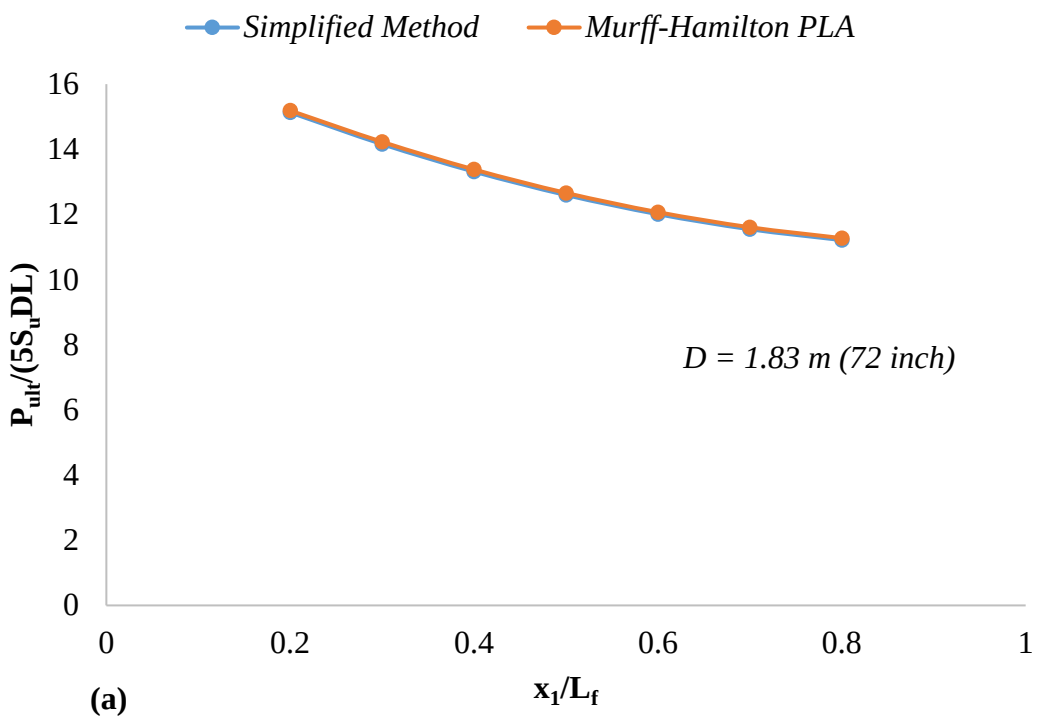

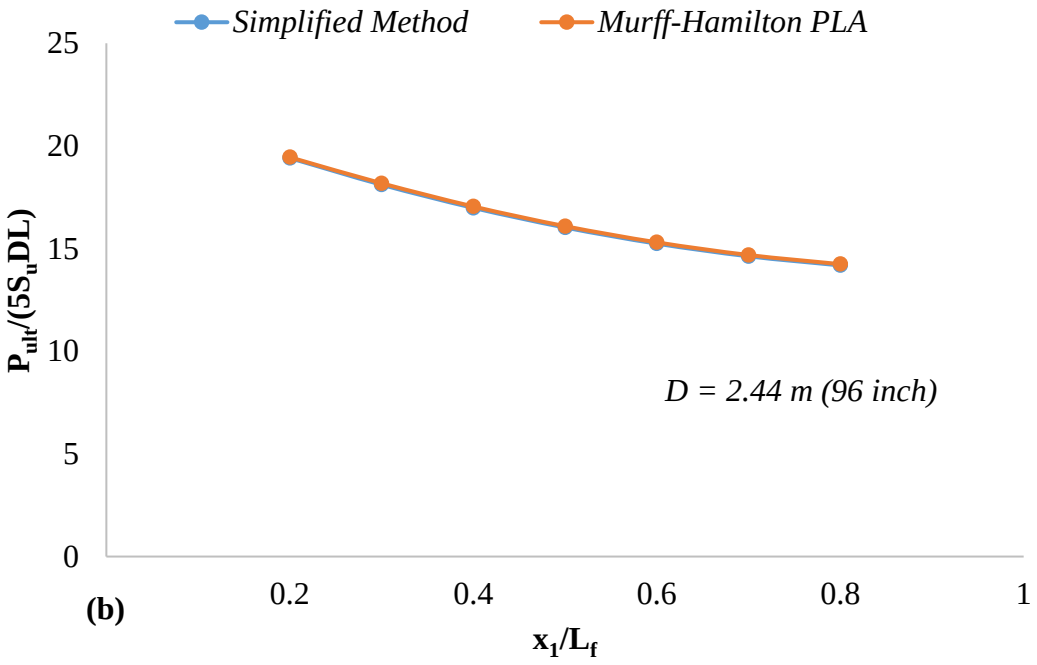

Figure 3.5: Normalized lateral capacity vs thickness ratio

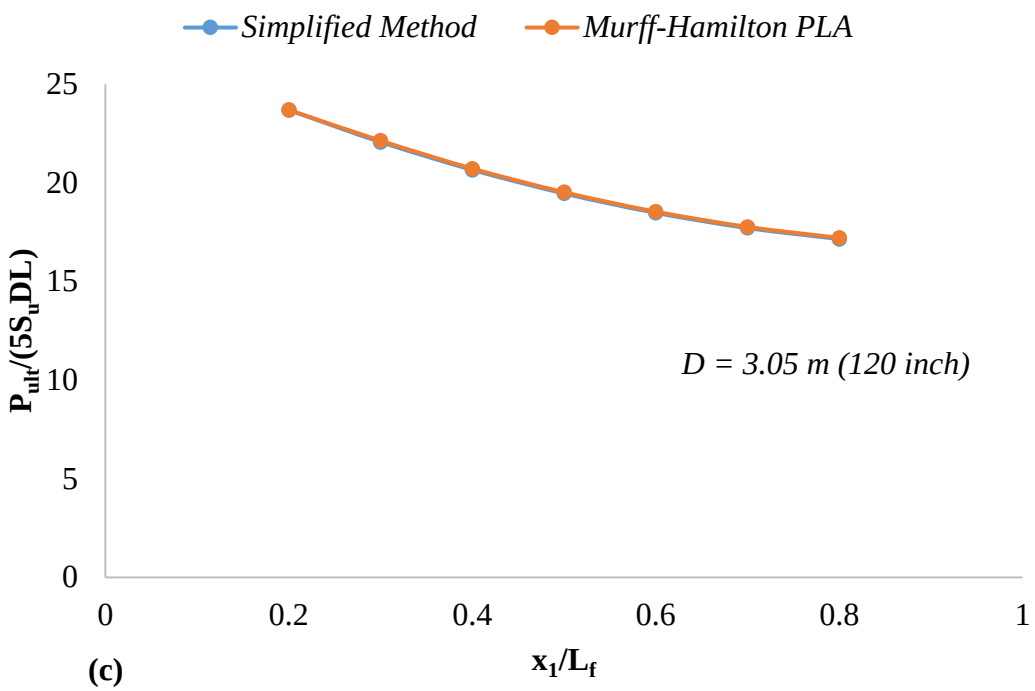

(c)

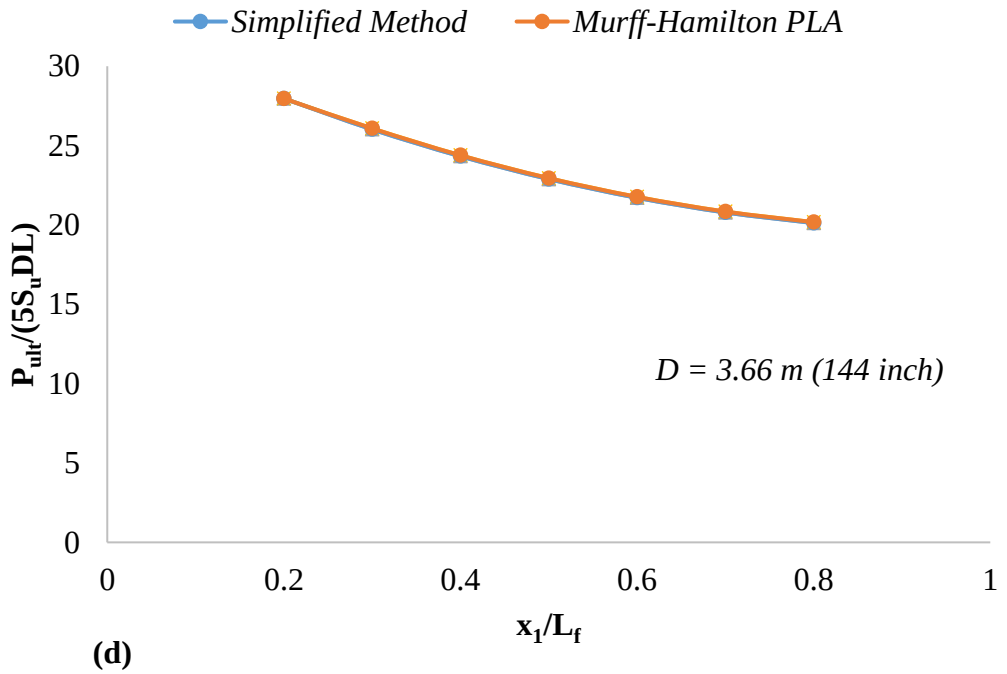

(d)

Figure 3.5 Continued.

3.7.3 Effect of Relative Gradient on Ultimate Capacity

To study the effect of change in relative gradient of the soil layers, variation in relative strength gradient form 20% of second layer to 300% (three times of second layer) was considered. To achieve this, second layer strength gradient (k_2) was varied such that the ratio k_1/k_2 changes from 0.2 to 3. The depth of layers was kept constant by fixing the first layer at 5m which is consistent with the soil data obtained for Gulf of Maine, as shown in Table 3.3. For all analyses, aspect ratio (L_f/D) of 6, and translating piles were considered.

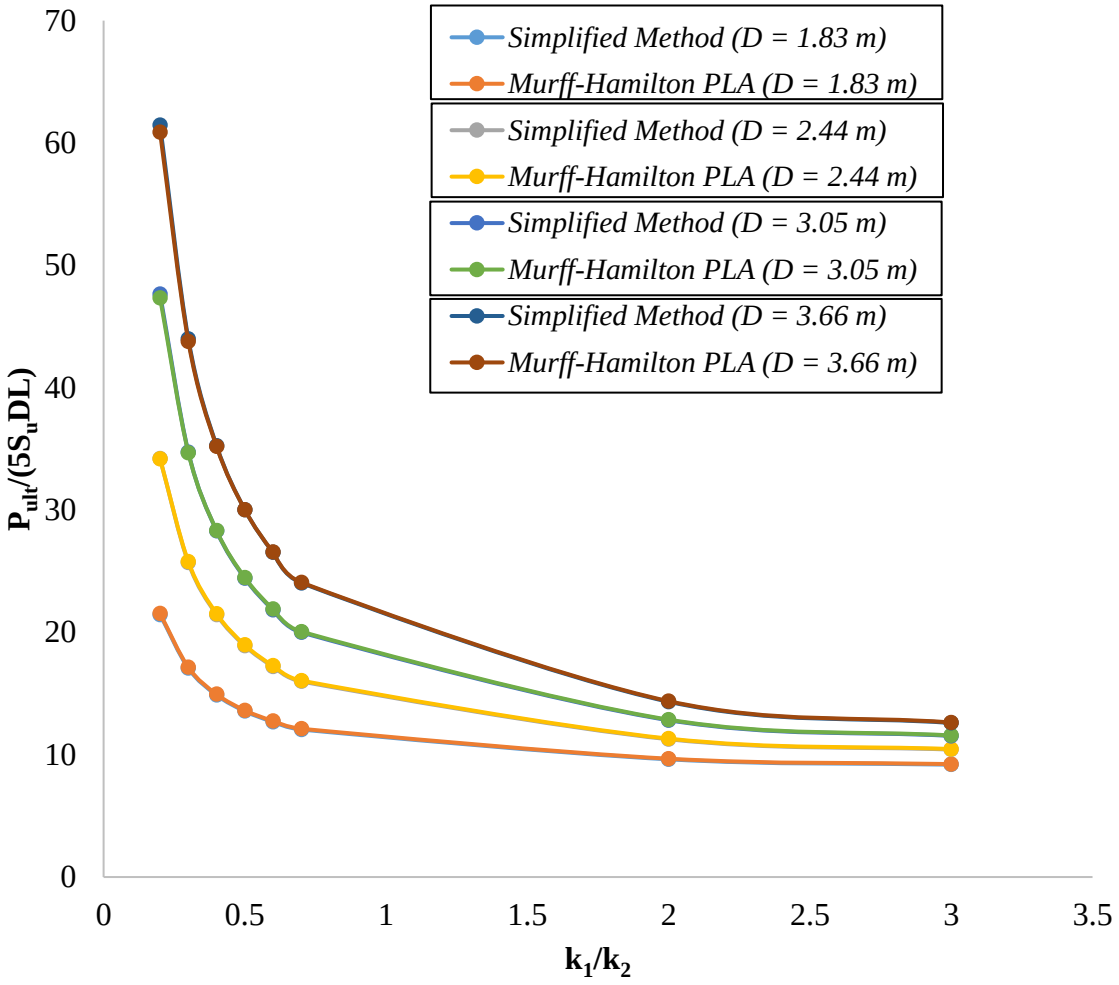

Figure 3.6: Normalized lateral capacity vs shear strength gradient ratio

Figure 3.6 shows the comparison of normalized lateral capacity as a function of relative strength gradient of soil. With the increase in pile diameter, the lateral capacity increases. With the increase in the ration (k_1/k_2), the normalized lateral capacity decreases. This can be attributed to decrease in overall shear strength of the soil since gradient of first layer is lower than the second layer. The results from both the analysis methods are very close and the plots result into overlapping curves.

3.7.4 Effect of Load Attachment Depth on Ultimate Capacity

Lateral capacity varies with the depth at which the mooring system is connected to caissons. Since the objective of this study is to validate the proposed methodology to analyze caisson in bilinear soil using Simplified Analysis, lateral capacity under different conditions, results considering varied load attachment depth was also needed to be compared.

Three load attachment depths (L_i) as 0, $2/3L_f$, and a depth corresponding to ultimate capacity (pure translation) was considered. The soil conditions as show in Table 3.3 were considered for the analyses. For all analyses, no gap behind the pile was considered.

Figure 3.7 shows the comparison of normalized lateral capacity varying with load attachment depth for both Simplified Method and Murff-Hamilton PLA. The capacity increases with increase in load attachment depth till it reaches the ultimate capacity.

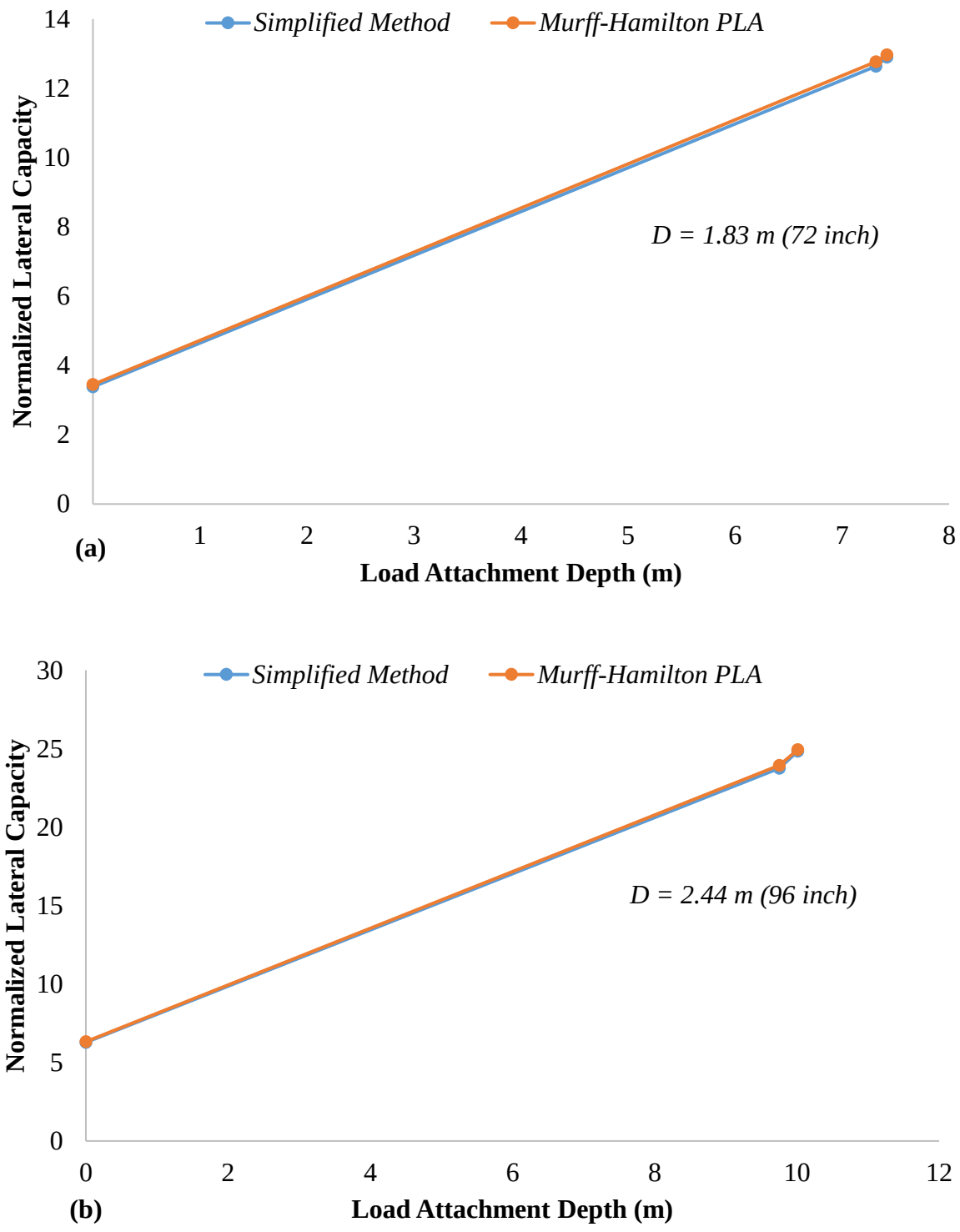

Figure 3.7: Normalized lateral capacity variation with load attachment depth (suction case)

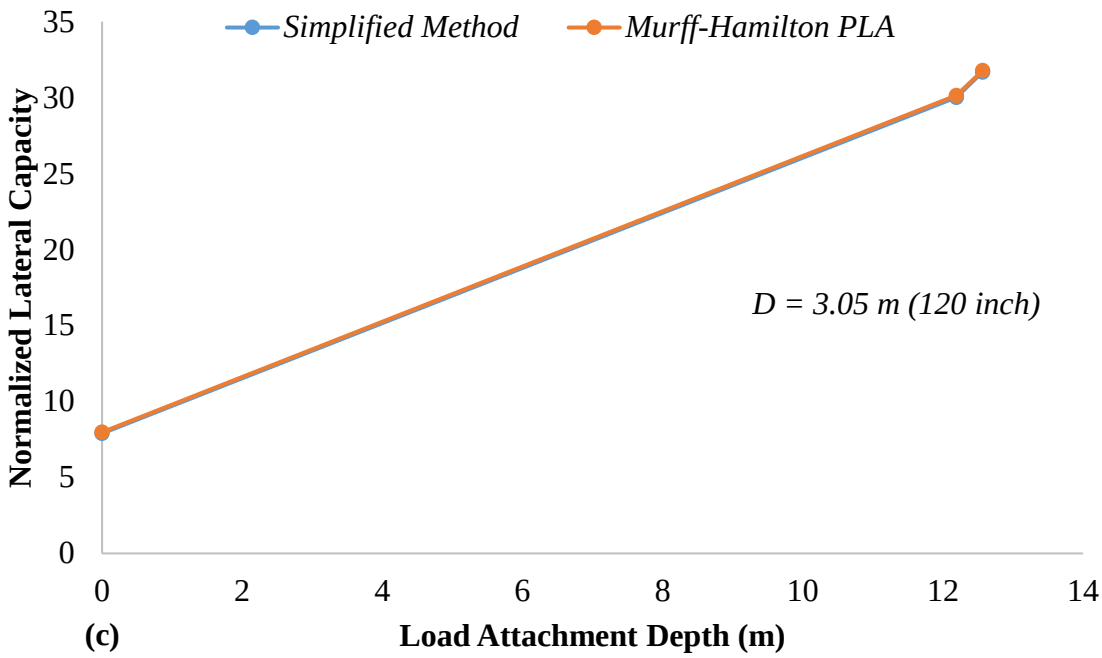

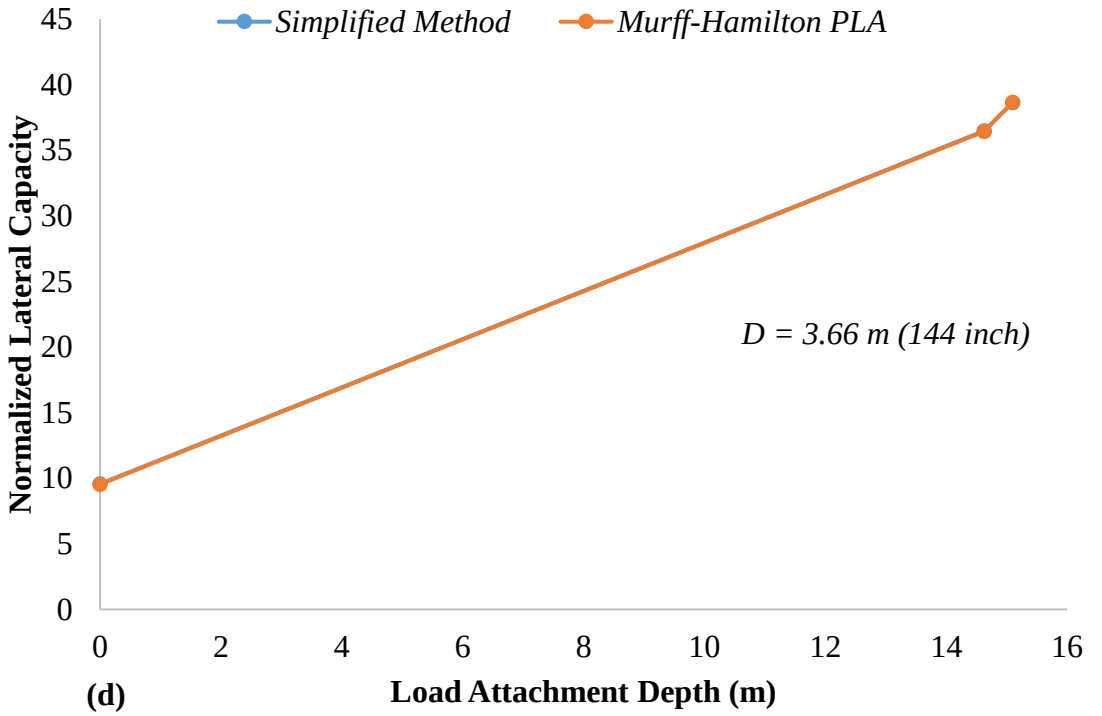

Figure 3. 7 Continued.

The pile corresponding to ultimate capacity is considered to be in pure translation. The results from both the analyses are in very close agreement and plotted in the form of overlapping lines.

3.7.5 No Suction

All the above analyses were carried out considering the full suction (no gap) behind the pile. Although, the soil considered is categorized as soft clay which means that a full suction is a correct assumption. However, in order to validate the applicability of the study to soils where a suction doesn't fully develop, gap formation was considered in the following analyses.

Three load attachment depths (L_i) as 0, $2/3L_f$, and depth corresponding to ultimate capacity (pure translation) was considered. The soil conditions as show in Table 3.3 were considered for the analyses, whereas an aspect ratio of 6 was considered for all the analyses.

Figure 3.8 shows the comparison of results from Simplified Method and Murff-Hamilton PLA. It can be seen that results from both the methods do not match as closely as they did for the suction case. The reason could be that for no suction, the effect of soil unit weight on the capacity is neglected. The assumption is very simplistic and there is a need to investigate soil unit weight effects on lateral capacity. The plots also show that with the increase in pile diameter, the difference between the ultimate capacities from both the analyses increases.

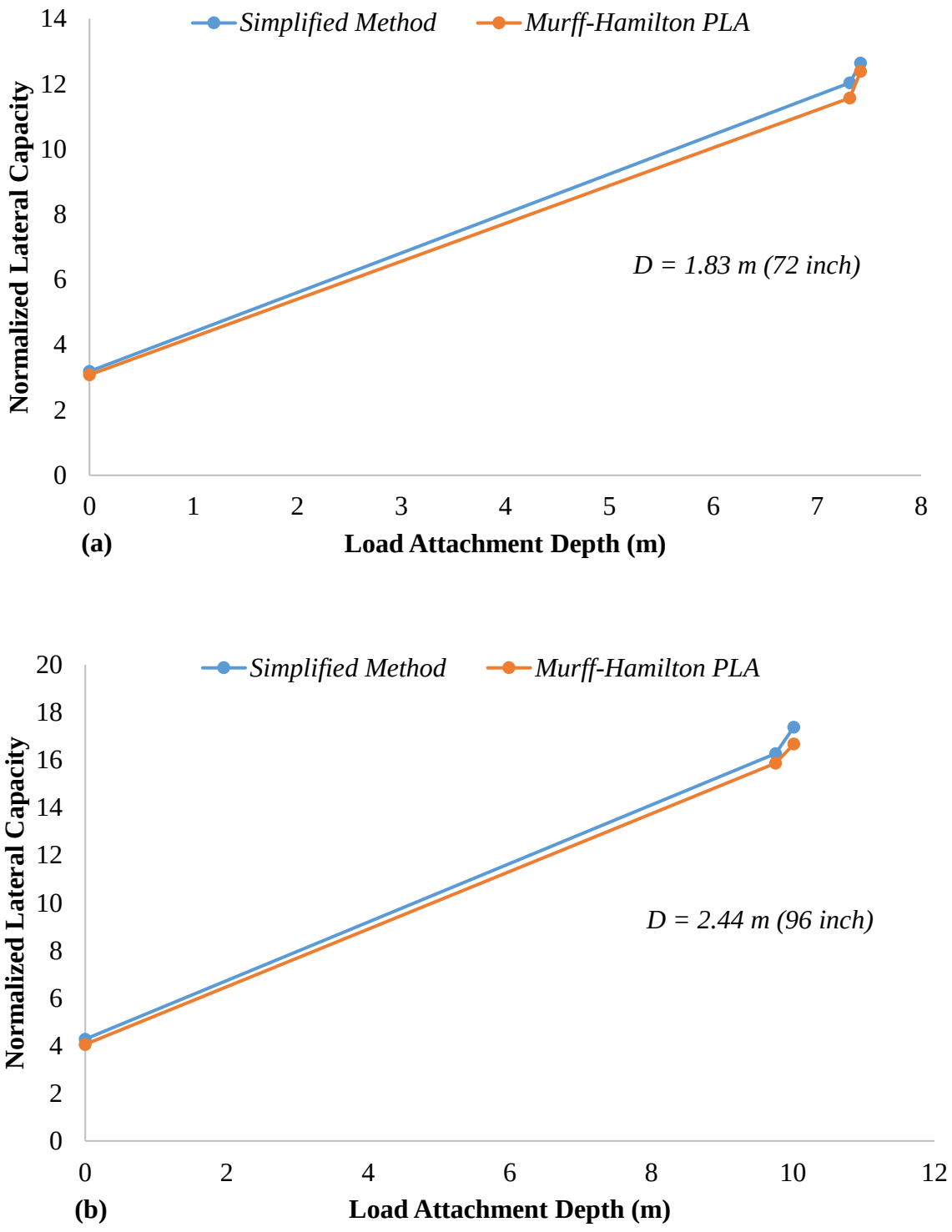

Figure 3.8: Normalized lateral capacity variation with load attachment depth (no suction case)

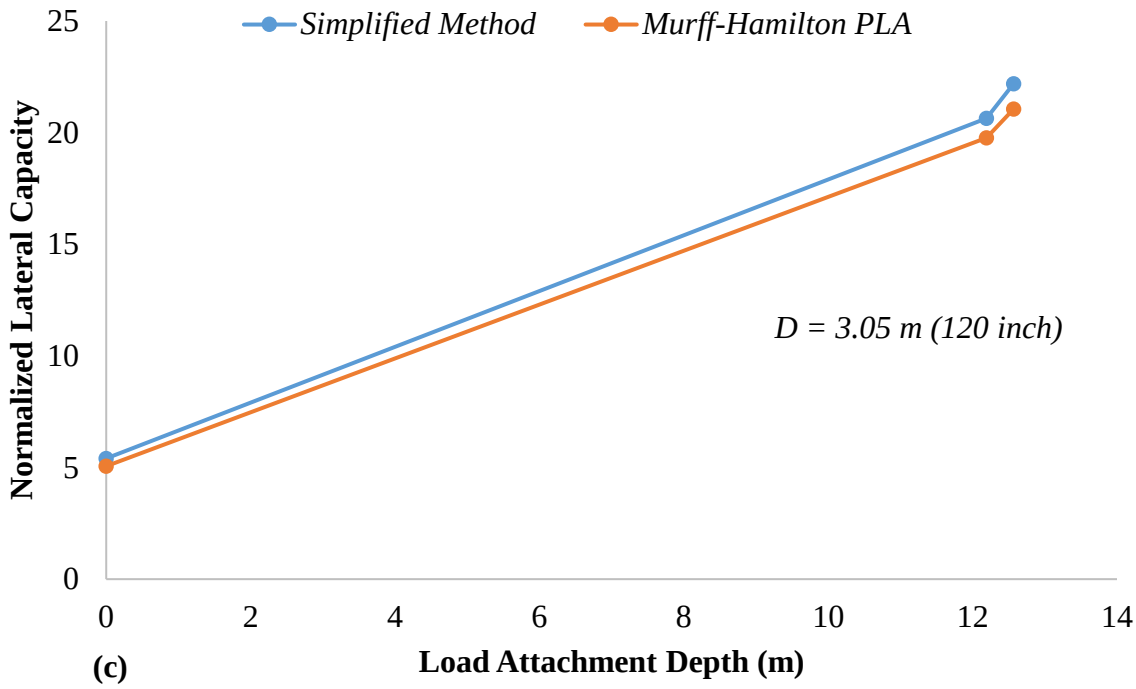

(c)

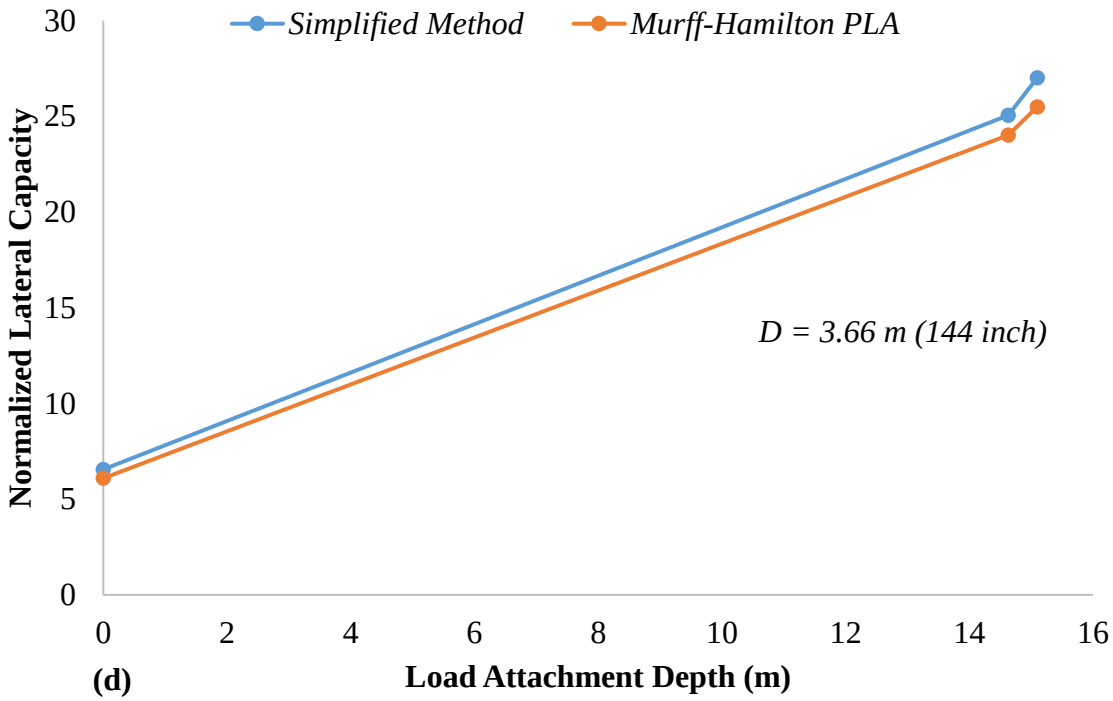

(d)

Figure 3.8 Continued.

4 SUMMARY AND CONCLUSIONS

4.1 Summary

Upper bound Plastic Limit Analysis (PLA) method to determine the collapse load of laterally load piles is a versatile tool capable to incorporate anisotropic soil conditions. However, the method requires significant computational energy as it involves computation of complex surface and volume integrals as well as optimization of four parameters which define the geometry of collapse mechanism. Therefore, the computational requirements for this method exceeds the capabilities of spreadsheet programs—which are highly desired in industry— and high programming skills are required to code it. Substantial simplification in the PLA is made by considering the net effect of the soil surrounding the caisson in terms of resultant forces and moments acting on the caisson. The expedient reduces the order of energy dissipation integrals from three to one, whereas the optimization parameters are reduced from four to one—hence called Simplified Method. The simplified method allows the computation to be carried out using spreadsheet programs; however, the method is limited to soil of uniform or linearly varying shear strength. Often, the soil strength profiles are complex than simple uniform or linearly varying with depth. One of the commonly found is a bilinear shear strength profile. This study is focused on devising a method which could convert bilinear profile into its equivalent linear so that the simplified method of analysis could be applied to pile in such soils.

4.2 Conclusions

The proposed methodology to convert bilinear shear strength profile into equivalent linear is based on equilibrium of net forces due to soil shear strength. For relatively short

stubby caissons (aspect ratio 2), Murff-Hamilton method yields higher collapse capacity with maximum difference of 3.6% among all caissons diameters. Overall, the analyses results obtained from both Simplified Method and Murff-Hamilton PLA closely match hence the resultant profile has proved to be a reliable representation of original soil shear strength. When analysis was carried out considering the variation in soil layer depth, overlapping results were obtained. Hence the methodology holds true for any combination of bilinear soil thicknesses. Minimal effect of relative gradient was observed. For the case of no suction behind the pile, a relatively large difference in results from both the analysis method is observed which is mainly due to reason that effect of unit weight is neglected in the analysis--which might not be completely true. Moreover, for no suction (gap) case, with the increase in diameter the difference in lateral capacities also increases.

4.3 Recommendation for Future Work

The study was carried out considering the soil profiles obtained from Gulf of Maine which can be categorized as Very Soft soil. Suction behind the pile is a reasonable assumption for the study. Therefore, the proposed methodology can be used for soils of similar nature. However, for firm soils a formation of gap is inevitable due to absence of suction hence further study is needed since the analyses show large difference in results for such soils. The proposed methodology was validated using Murff-Hamilton PLA which itself has some limitations e.g. it overestimates the capacity for short piles. Therefore, it is recommended to validate the study using finite element (FE) modeling.

REFERENCES

Arapogianni, A., Genachte, A., Ochagavia, R. M., Vergara, J., Castell, D., Tsouroukdissian, A. R., Schuon, F. (2013). Deep Water; The next step for offshore wind energy. *European Wind Energy Association (EWEA), Brussels, Belgium, ISBN*, 978-972.

Aubeny, C., & Murff, J. D. (2005). Simplified limit solutions for the capacity of suction anchors under undrained conditions. *Ocean Engineering, 32*(7), 864-877.

Aubeny, C., Han, S.-W., & Murff, J. D. (2003). Suction caisson capacity in anisotropic, purely cohesive soil. *International Journal of Geomechanics, 3*(2), 225-235.

Aubeny, C., Murf, J., & Moon, S. (2001). *Lateral undrained resistance of suction caisson anchors.* (11), (03)

Baglioni, V. P., Chow, G. S., & Endley, S. N. (1982). *Jack-up rig foundation stability in stratified soil profiles.* Paper presented at the Offshore Technology Conference.

Bai, Y., & Bai, Q. (2012). *Subsea engineering handbook*: Gulf Professional Publishing.

Bang, S., Jones, K., Kim, K., Kim, Y., & Cho, Y. (2011). Inclined loading capacity of suction piles in sand. *Ocean Engineering, 38*(7), 915-924.

Broms, B. B. (1964). Lateral resistance of piles in cohesive soils. *Journal of the Soil Mechanics and Foundations Division, 90*(2), 27-64.

Chakrabarty, J. (2012). *Theory of plasticity*: Butterworth-Heinemann.

Duncan, J. M., & Chang, C.-Y. (1970). Nonlinear analysis of stress and strain in soils. *Journal of Soil Mechanics & Foundations Div*.

Gerwick Jr, B. (2000). Construction of marine and offshore structures, CRC Press.

Heyman, J. (1972). *Coulomb's memoir on statics: an essay in the history of civil engineering*: CUP Archive.

Hill, R. (1998). *The mathematical theory of plasticity* (Vol. 11): Oxford university press.

Houlsby, G. T. (1981). *Study of plasticity theories and their applicability to soils.* University of Cambridge,

Koutsoftas, D. C., Foott, R., & Handfelt, L. D. (1987). Geotechnical investigations offshore Hong Kong. *Journal of Geotechnical Engineering, 113*(2), 87-105.

Li, D., Zhang, Y., Feng, L., & Gao, Y. (2015). Capacity of modified suction caissons in marine sand under static horizontal loading. *Ocean Engineering, 102*, 1-16.

Matlock, H. (1970). Correlations for design of laterally loaded piles in soft clay. *Offshore technology in civil engineering's hall of fame papers from the early years*, 77-94.

Murff, J. D., & Hamilton, J. M. (1993). *P-ultimate for undrained analysis of laterally loaded piles.* (119), (1)

Randolph, M. F., & Houlsby, G. (1984). The limiting pressure on a circular pile loaded laterally in cohesive soil. *Geotechnique, 34*(4), 613-623.

Randolph, M. F., & Houlsby, G. (1984). The limiting pressure on a circular pile loaded laterally in cohesive soil. *Geotechnique, 34*(4), 613-623.

Randolph, M., Gourvenec, S., White, D., & Cassidy, M. (2011). *Offshore geotechnical engineering* (Vol. 2): Spon Press New

Roddier, D., Cermelli, C., Aubault, A., & Weinstein, A. (2010). WindFloat: A floating foundation for offshore wind turbines. *Journal of renewable and sustainable energy, 2*(3), 033104.

Sættem, J., Rise, L., Rokoengen, K., & By, T. (1996). Soil investigations, offshore mid Norway: A case study of glacial influence on geotechnical properties. *Global and Planetary Change, 12*(1), 271-285. doi:https://doi.org/10.1016/0921-8181(95)00024-0

Schofield, A., & Wroth, P. (1968). *Critical state soil mechanics* (Vol. 310): McGraw-Hill London.

York.

Young, A. G., Remmes, B. D., & Meyer, B. J. (1984). Foundation performance of offshore jack-up drilling rigs. *Journal of Geotechnical Engineering, 110*(7), 841-859.

Yu, M.-h. (2002). Advances in strength theories for materials under complex stress state in the 20th century. *Applied Mechanics Reviews, 55*(3), 169-218.

APPENDIX A

EQUIVALENT STRENGTH FUNCTION

```
%CODE TO COVERT BILINEAR PROFILE INTO EQUIVALENT LINEAR

% layer boundary depth
x1=5;
% caisson depth
% Lf=6*D;
x2=Lf-x1;
% % strength of upper layer
Su01=40;
k1=1.5;
% strength of lower layer
Su02=Su01+k1*x1;   %strength at top of lower layer
k2=2;
% compute resultant force
A(1)=Su01*x1;
A(2)=k1*x1^2/2;
A(3)=Su02*x2;
A(4)=k2*x2^2/2;
R=sum(A);
% compute resultant moment
M(1)=A(1)*x1/2;
M(2)=A(2)*2*x1/3;
M(3)=A(3)*(x1+x2/2);
M(4)=A(4)*(x1+2*x2/3);
Mr=sum(M);
xbar=Mr/R;
% compute equivalent linear profile
su0_side=Su01;
k_side=2*(R-Su01*Lf)/Lf^2;
%strength profile for tip resistance calculations
su0_tip=Su02+(Lf-x1)*k2;
k_tip=k2;
su01=su0_side;        %mudline strength, side of caisson
k=k_side;             %strength gradient, side of caisson
su02=su0_tip;         %strength at tip
k2=k_tip;             %strength gradient below tip of caisson
```

APPENDIX B

NORMALIZED BEARING CAPACITY PLOTS

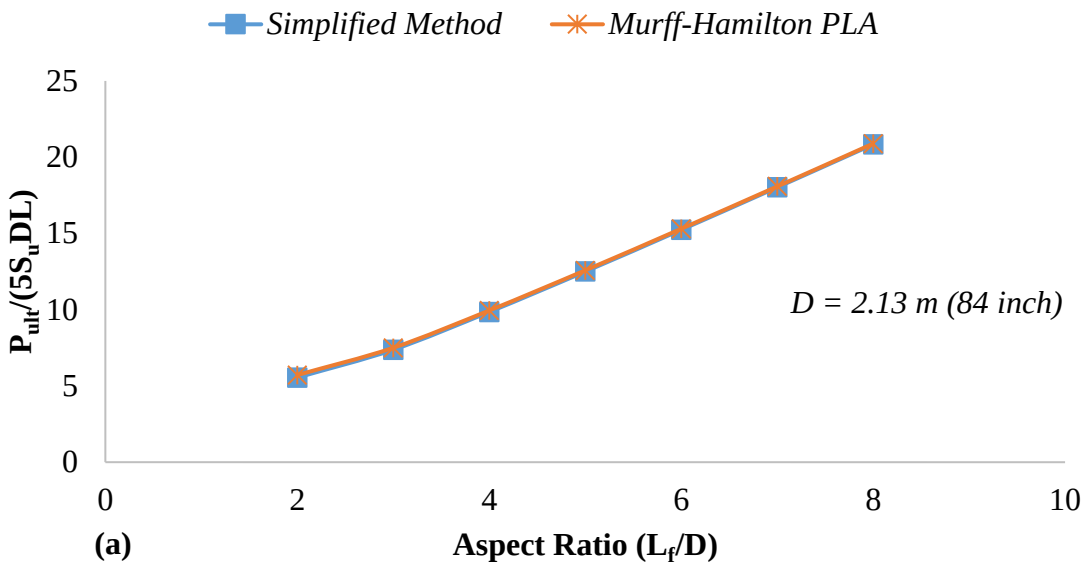

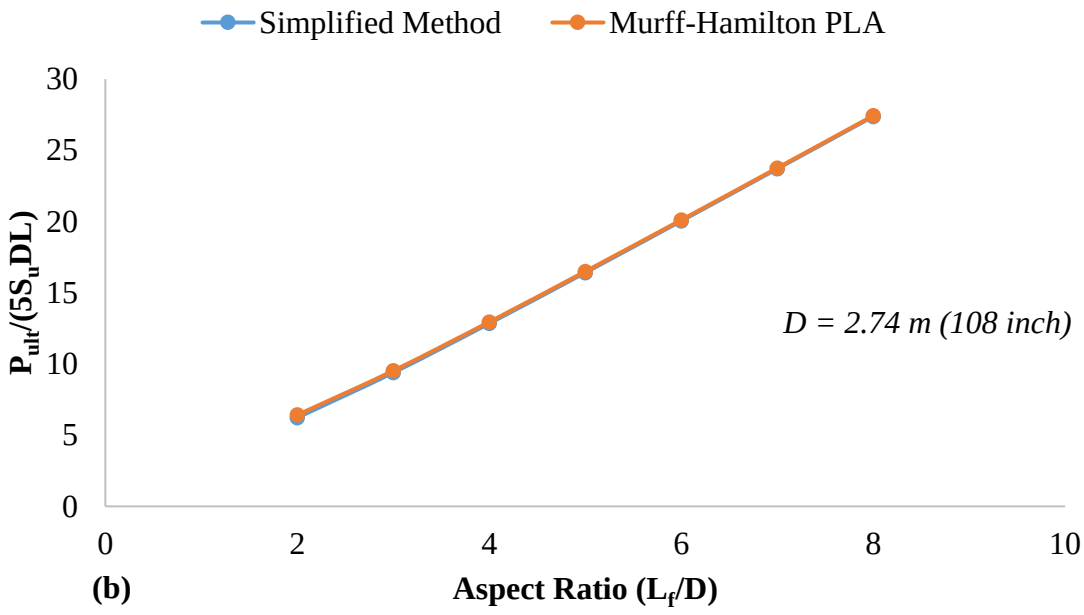

Figure B 1: Normalized lateral capacity for different aspect ratios

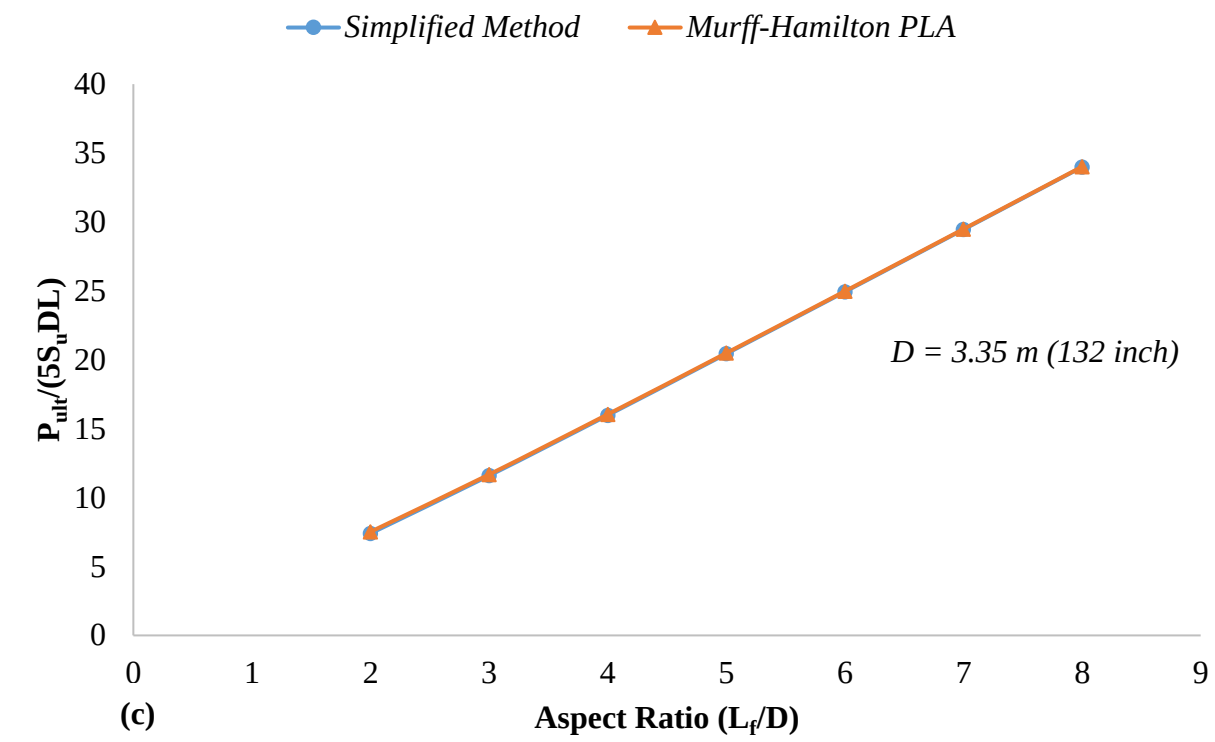

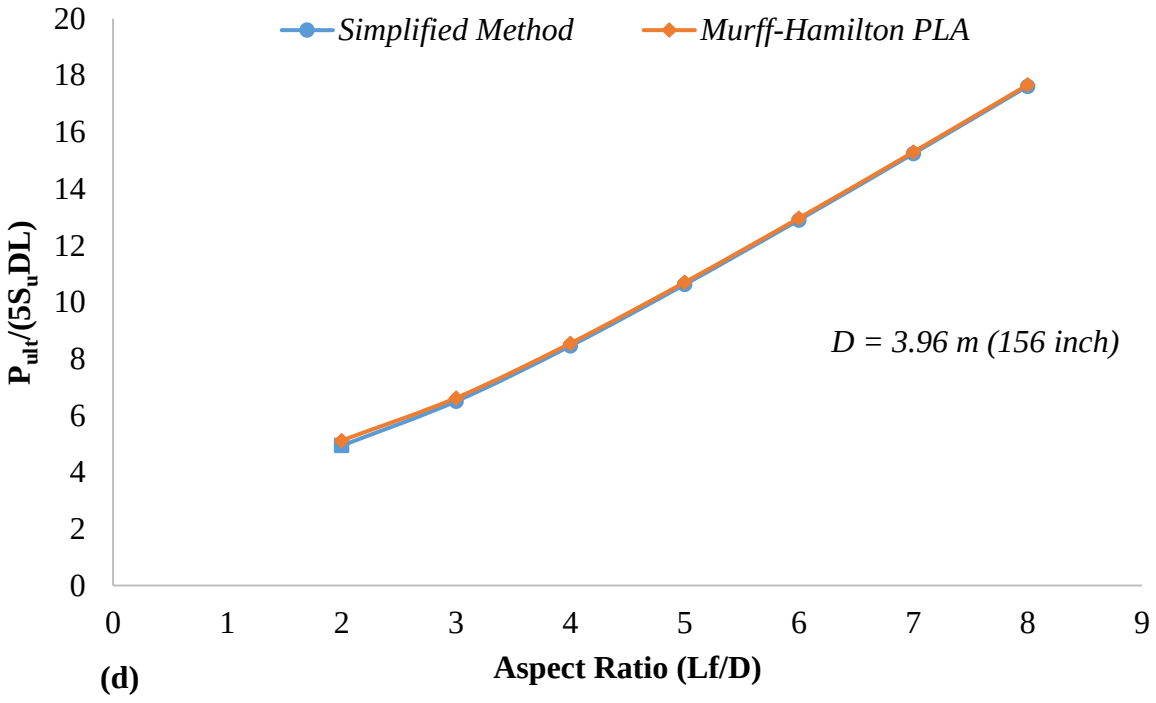

Figure B 1 Continued.

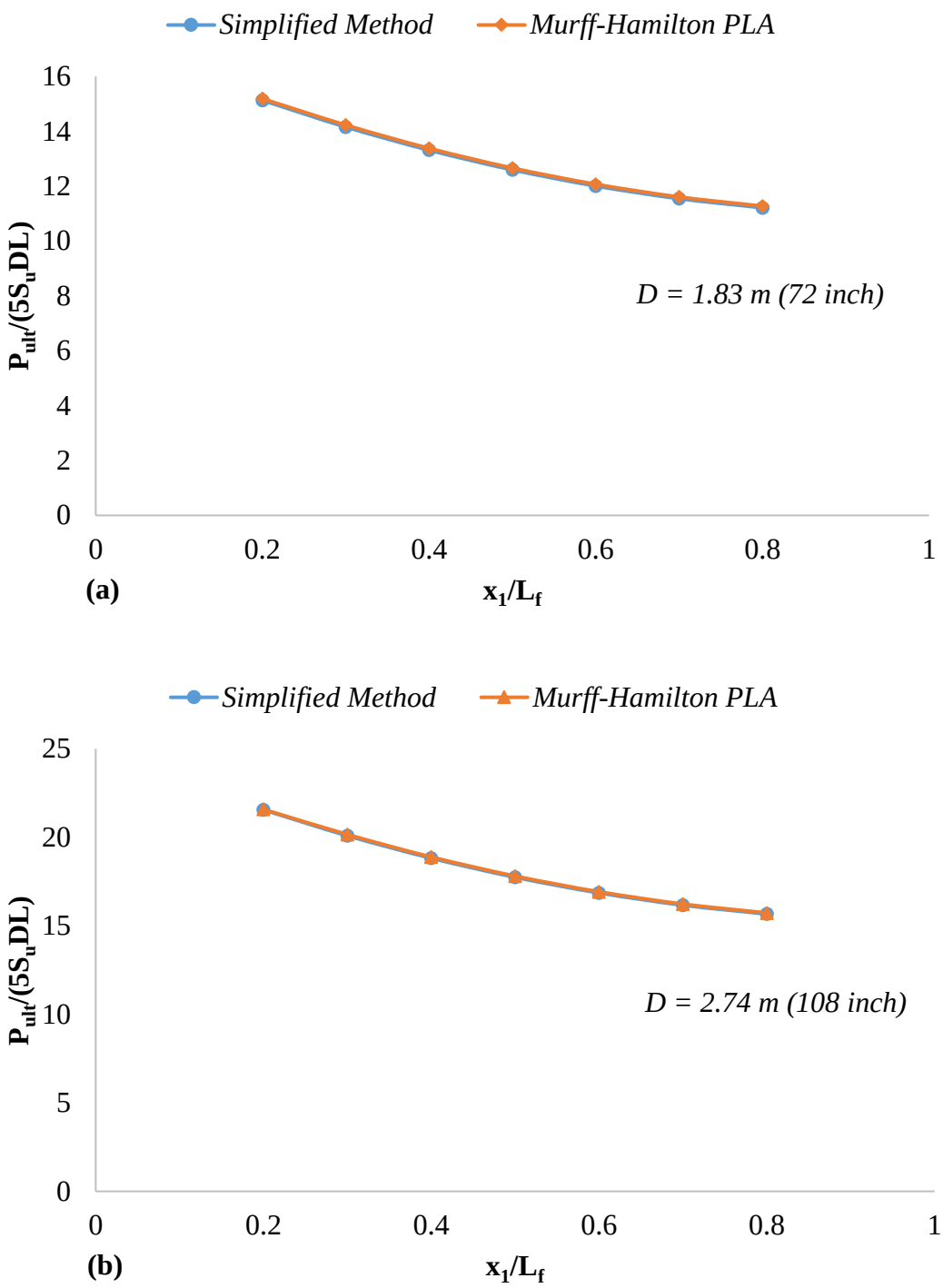

Figure B 2: Normalized lateral capacity vs thickness ratio

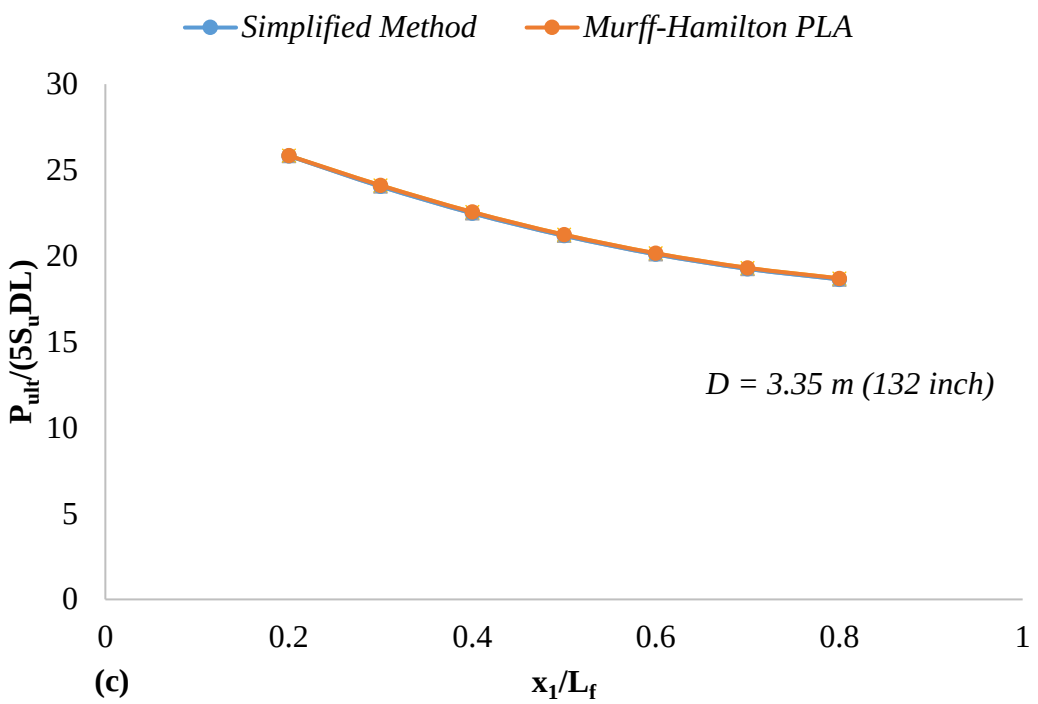

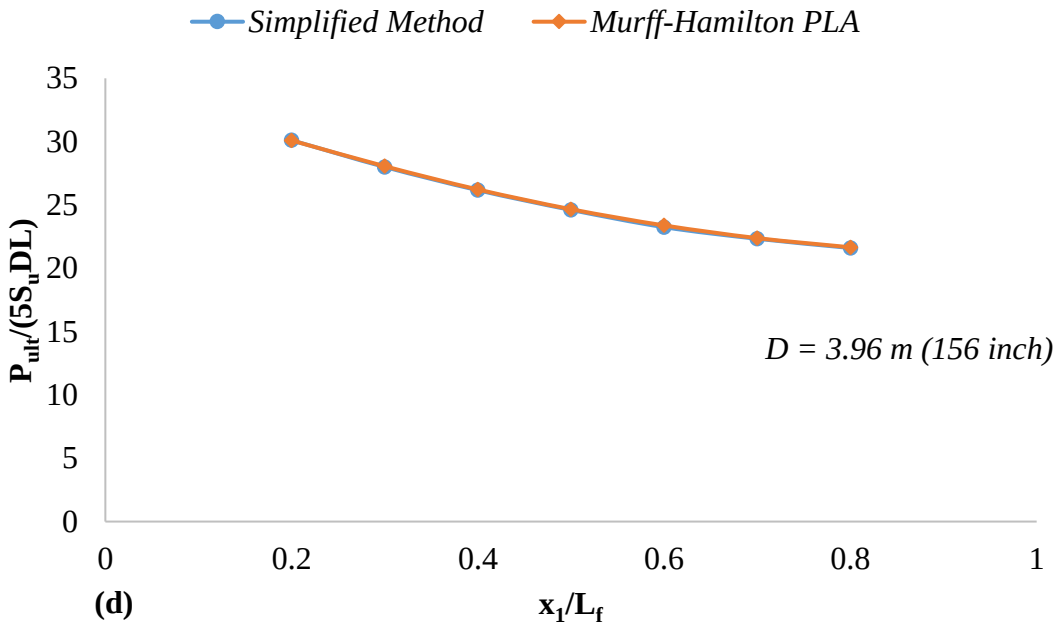

Figure B 2 Continued.

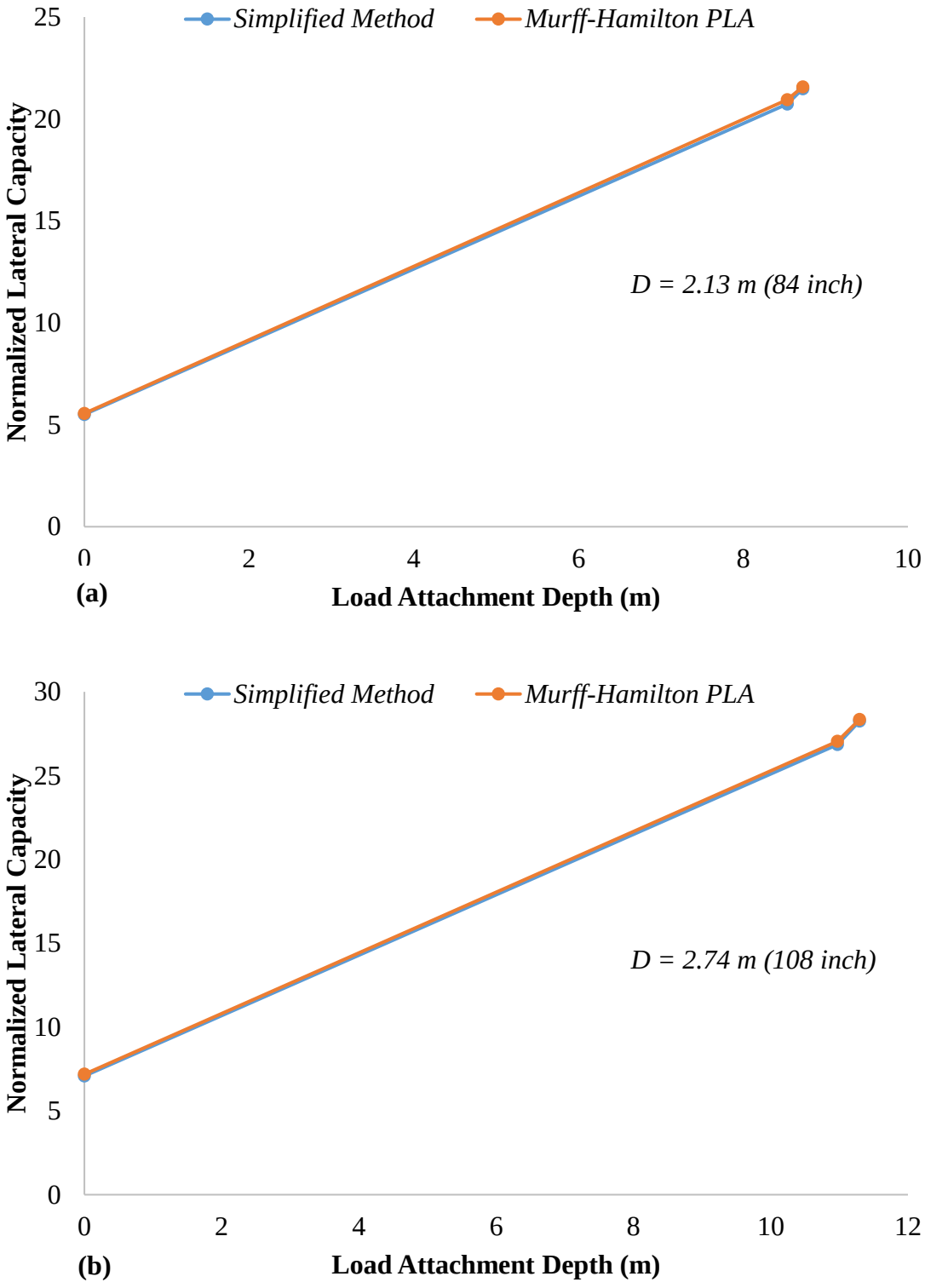

Figure B 3: Normalized lateral capacity variation with load attachment depth (suction case)

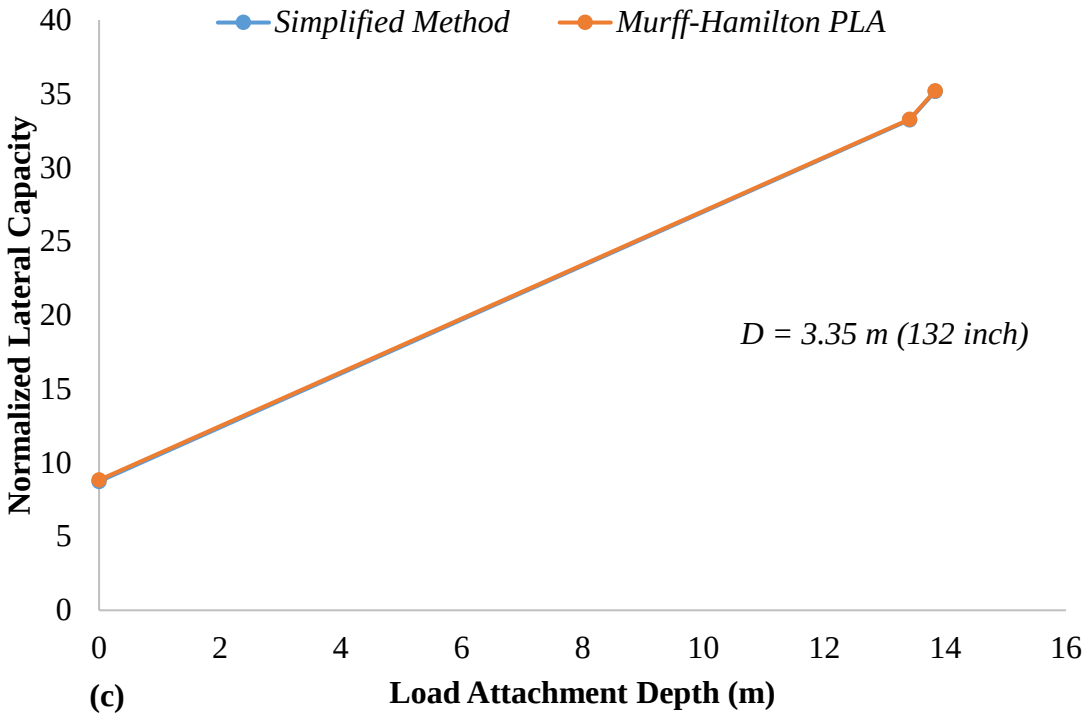

(c)

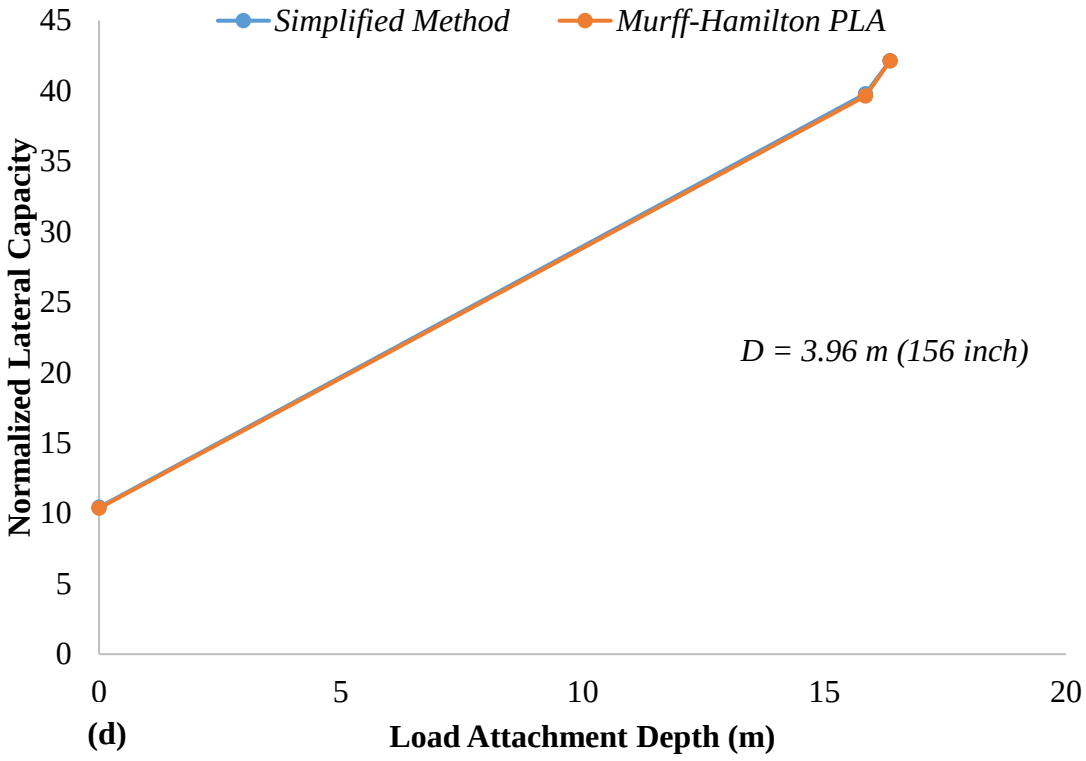

(d)

Figure B 3 Continued.